OPEN ACCESS
Fractals, Vol. 31, No. 10 (2023) 2340087 (22 pages)

DOI: 10.1142/S0218348X2340087X

NUMERICAL ANALYSIS FOR HIDDEN CHAOTIC BEHAVIOR OF A COUPLED MEMRISTIVE DYNAMICAL SYSTEM VIA FRACTAL–FRACTIONAL OPERATOR BASED ON NEWTON POLYNOMIAL INTERPOLATION

SHAIMAA A. M. ABDELMOHSEN,[*] SHABIR AHMAD,[†,§§,‖‖] MANSOUR F. YASSEN,[‡,§] SAEED AHMED ASIRI,[¶] ABDELBACKI M. M. ASHRAF,[‖] SAYED SAIFULLAH[†] and FAHD JARAD[**,††,‡‡,¶¶,‖‖]

*[*]Department of Physics, College of Science
Princess Nourah Bint Abdulrahman University
P.O. Box 84428, Riyadh 11671, Saudi Arabia*

*[†]Department of Mathematics, University of Malakand
Chakdara, Dir Lower, Khyber Pakhtunkhwa, Pakistan*

*[‡]Department of Mathematics
College of Science and Humanities in Al-Aflaj
Prince Sattam Bin Abdulaziz University
Al-Aflaj 11912, Saudi Arabia*

*[§]Department of Mathematics, Faculty of Science
Damietta University
New Damietta 34517, Damietta, Egypt*

[‖‖]Corresponding authors.

¶Mechanical Engineering Department
Engineering College, King Abdulaziz University
Jeddah, Saudi Arabia

‖Plant Pathology Department, Faculty of Agriculture
Cairo University, Giza 12613, Egypt

**Department of Mathematics, Cankaya University
Etimesgut 06790, Ankara, Turkey

††Department of Mathematics, King Abdulaziz University
Jeddah 21589, Saudi Arabia

‡‡Department of Medical Research
China Medical University, Taichung 40402
Taiwan, R. O. China

§§shabirahmad2232@gmail.com
¶¶fahd@cankaya.edu.tr

Received March 11, 2022
Accepted December 5, 2022
Published September 23, 2023

Abstract

Dynamical features of a coupled memristive chaotic system have been studied using a fractal–fractional derivative in the sense of Atangana–Baleanu. Dissipation, Poincaré section, phase portraits, and time-series behaviors are all examined. The dissipation property shows that the suggested system is dissipative as long as the parameter $g > 0$. Similarly, from the Poincaré section it is observed that, lowering the value of the fractal dimension, an asymmetric attractor emerges in the system. In addition, fixed point notions are used to analyze the existence and uniqueness of the solution from a fractal–fractional perspective. Numerical analysis using the Adams–Bashforth method which is based on Newton's Polynomial Interpolation is performed. Furthermore, multiple projections of the system with different fractional orders and fractal dimensions are quantitatively demonstrated, revealing new characteristics in the proposed model. The coupled memristive system exhibits certain novel, strange attractors and behaviors that are not observable by the local operators.

Keywords: Dissipation; Asymmetric Attractor; Adams–Bashforth Method.

1. INTRODUCTION

The presence of a memristor was predicted by Chua in 1971. It has received a lot of interest in academic and engineering circles as the fourth electrical device to emerge, following resistance, capacitance, and inductance. Artificial neural morphology networks, brain-like computation, private communications, and novel memory are only a few of the applications.[1–3] Because of the memristor's unique nonlinear properties, integrating it with other parts makes it simple to build a chaotic oscillation circuit and a neural morphology circuit. There seem to be several methods to build these chaotic oscillatory circuits.[4,5] In recent years, using a mathematical model of a memristor to examine a coupled memristive system has become popular. The majority of research focuses on the synchronization of linked systems. Nonetheless, memristor-to-circuit coupling research is uncommon. There are only a few studies that demonstrate coupling in circuit mode. The literature[6] developed a dynamical system focusing on the linked Chua's circuit and showed that chaotic traveling wave solutions occur for that kind of system. Researchers in Ref. 7 thoroughly investigated the circuit behavior of Chua's cycle with memory using a series-coupled Chua's circuit of similar polarity memristor. By linking a magnetic flux-controlled memristor with the RCL shunted junction circuit, as discussed in the source,[8] a novel four-dynamical system is developed. The system might be applied to control the chaotic circuit, which consists of a memristor and a Josephson transistor. Two memristors, one of which is a feedback coupling memristor, make up the chaotic circuit systems.[9,10]

Contrasting the self-excited attractor,[11] researchers like Leonov *et al.* discovered a new form of attractor called hidden attractors, whose basins do not meet at an unstable equilibrium point. The development of this novel sort of attractor has sparked the interest of academics. For a hidden chaotic system, there are an unlimited number of equilibrium points (EPs),[12] just one stable equilibrium point,[13] or no equilibrium point.[14] The use of memristors in nonlinear circuit systems is growing thanks to the emergence of memristors and the expanding variety of models available. Nevertheless, the majority of these investigations[15] have concentrated on self-excited attractor attractors. In the memristive hidden chaotic systems, there have been a few reports of systems lacking an equilibrium point. A delayed memristive chaotic system with no equilibrium point was presented in Ref. 16, and a dynamic behavior investigation was conducted. A memristive hidden attractor with no equilibrium point was defined in Ref. 17, and its features, including coexisting bifurcation and multistability, were investigated. However, the existence of a double memristive hidden circuit system centered on coupled memristors without an equilibrium point has yet to be revealed. Very recently, Du *et al.*[18] introduced a double memristive model with no equilibrium point as follows:

$$\begin{cases} \dfrac{d\mathbb{X}(t)}{dt} = \kappa\mathbb{Y}, \\ \dfrac{d\mathbb{Y}(t)}{dt} = \varepsilon(-\mathbb{X} - \sigma\mathbb{Y}\mathbb{Z}), \\ \dfrac{d\mathbb{Z}(t)}{dt} = \varsigma + \gamma|\mathbb{Z}| + \delta\mathbb{Y}^2, \\ \dfrac{d\mathbb{W}(t)}{dt} = -g(m + n|\mathbb{V}|)\mathbb{W} + \mathbb{Z}\mathbb{W} + e, \\ \dfrac{d\mathbb{V}(t)}{dt} = \mathbb{W} - \mathbb{V}. \end{cases} \tag{1}$$

Modeling with local operators fails when memory and complex behavior of a problem are taken into account. Nonlocal operators have the ability to handle issues related to memory features and complex behavior of a physical phenomenon. Due to their tendency to incorporate extra complicated physical events into mathematical terms, the concept of fractional operators has drawn numerous scientists from practically every discipline of applied sciences at present.[19–21] So far, three kernels, such as the power kernel, exponential decay kernel, and generalized Mittag-Leffler kernel, have all been offered as prepotent in this discipline. With the use of these kernels, the three most important operators were defined in the literature. The most fundamental one is the Caputo operator, which is defined in the power-law kernel. After some decades, Caputo and Fabrizio introduced a nonsingular operator by using an exponential decay kernel. In 2016, with the help of the generalized Mittag-Leffler law, Atangana and Baleanu defined another type of fractional operator. These operators have been frequently used in the modeling of different physical problems. To generalize the nonlocal operators with different kernels, in 2017, Atangana constructed new differential and integral operators by integrating fractional calculus with fractal calculus,[22] which we call fractal–fractional operators (FFOs). Memory influence, heterogeneity, and elasto-viscosity of a medium, as well as the fractal structure of a dynamic model, are all taken into consideration by these operators. FFOs have been implemented to many real-world problems that occur in various fields of sciences. For instance, a Drinfeld–Sokolov–Wilson model has been studied via nonsingular FFOs.[23] Aslam *et al.* proposed a chemistry kinetics hires problem via FFO.[24] FFO operator has also a key role in the analysis of hidden attractors. For example, Saifullah and coworkers analyzed the complex hidden attractors of a dynamical model via FFOs.[25] The nonsingular FFO was used in Ref. 26 to demonstrate the hidden attractors of Bhalekar–Gejji dynamical system. Zhang *et al.* investigated some new features of a chaotic system with one signum function under FFO.[27] Some interesting works on fractal–fractional chaotic systems are given in Refs. 28 and 29. Inspired by the above literature, we study system (1) under FFO with the Mittag-Leffler kernel. The above model (1) in the sense of fractal–fractional operator having the

Mittag-Leffler kernel is considered as

$$\begin{cases} {}^{\mathrm{MLK}}D_t^{\varpi,\varrho}(\mathbb{X}) = \kappa\mathbb{Y}, \\ {}^{\mathrm{MLK}}D_t^{\varpi,\varrho}(\mathbb{Y}) = \varepsilon(-\mathbb{X} - \sigma\mathbb{Y}\mathbb{Z}), \\ {}^{\mathrm{MLK}}D_t^{\varpi,\varrho}(\mathbb{Z}) = \varsigma + \gamma|\mathbb{Z}| + \delta\mathbb{Y}^2, \\ {}^{\mathrm{MLK}}D_t^{\varpi,\varrho}(\mathbb{W}) = -g(m + n|\mathbb{V}|)\mathbb{W} + \mathbb{Z}\mathbb{W} + e, \\ {}^{\mathrm{MLK}}D_t^{\varpi,\varrho}(\mathbb{V}) = \mathbb{W} - \mathbb{V}, \end{cases} \tag{2}$$

where ϖ and ϱ represent fractional order and fractal dimension, respectively. System (2) has four nonlinear terms including one quadratic nonlinearity. In the above model, e is constant, m, g, and n are the positive coefficients of the memristors, and $\mathbb{W}(\mathbb{V}) = gm + gn|\mathbb{V}|$.

In this paper, we study the considered coupled memristive system using a fractal–fractional operator under the nonlocal and nonsingular kernel. We demonstrate the time-series and phase portraits of the considered system for few values of fractional order and fractal dimension. Also, we study the existence and uniqueness of a solution and the numerical results of the considered model. Now, we give the definitions of FFO with Mittag-Leffler kernel and its associated integral.

Definition 1 (Ref. 30). Let $\mathscr{G}(t)$ in (a, b) be a continuous function, then the fractal–fractional derivative in the sense of ABC is given as

$${}^{\mathrm{ABC}}\mathcal{D}^{\varpi,\varrho}(\mathscr{G}(t)) = \frac{\mathrm{AB}(\varpi)}{1-\varpi}\int_0^t \frac{d}{d\wp^{\varrho}}\mathscr{G}(\wp)\sigma_{\varpi} \times \left[\frac{-\varpi}{1-\varpi}(t-\wp)^{\varpi}\right]d\wp, \tag{3}$$

where the normalization function can be $\mathrm{AB}(0) = \mathrm{AB}(1) = 1$.

Definition 2 (Ref. 30). Suppose a function $\mathscr{G}(t)$ in (a, b) be continuous with arbitrary order $0 < \varpi \leq 1$ and fractal dimension $0 < \varrho \leq 1$ in the ABC sense that is given as

$${}^{\mathrm{ABC}}\mathcal{I}_0^{\varpi,\varrho}(\mathscr{G}(t)) = \frac{1-\varpi}{\mathrm{AB}(\varpi)}t^{\eta-1}\mathscr{G}(t) + \frac{\varrho\varpi}{\mathrm{AB}(\varpi)\Gamma(\varpi)}\int_0^t (t-\wp)^{\varpi-1} \times \wp^{\varrho-1}\mathscr{G}(\wp)d\wp. \tag{4}$$

2. EXISTENCE AND UNIQUENESS

Here, we will use the fixed point results to prove the existence and uniqueness of our proposed model,

$$\begin{cases} {}^{\mathrm{ABC}}\mathcal{D}_t^{\varpi}\mathbb{X}(t) = \varrho t^{\varrho-1}\mathbb{U}_1(t, \mathbb{X}, \mathbb{Y}, \mathbb{Z}, \mathbb{W}, \mathbb{V}), \\ {}^{\mathrm{ABC}}\mathcal{D}_t^{\varpi}\mathbb{Y}(t) = \varrho t^{\varrho-1}\mathbb{U}_2(t, \mathbb{X}, \mathbb{Y}, \mathbb{Z}, \mathbb{W}, \mathbb{V}), \\ {}^{\mathrm{ABC}}\mathcal{D}_t^{\varpi}\mathbb{Z}(t) = \varrho t^{\varrho-1}\mathbb{U}_2(t, \mathbb{X}, \mathbb{Y}, \mathbb{Z}, \mathbb{W}, \mathbb{V}), \\ {}^{\mathrm{ABC}}\mathcal{D}_t^{\varpi}\mathbb{W}(t) = \varrho t^{\varrho-1}\mathbb{U}_1(t, \mathbb{X}, \mathbb{Y}, \mathbb{Z}, \mathbb{W}, \mathbb{V}), \\ {}^{\mathrm{ABC}}\mathcal{D}_t^{\varpi}\mathbb{V}(t) = \varrho t^{\varrho-1}\mathbb{U}_1(t, \mathbb{X}, \mathbb{Y}, \mathbb{Z}, \mathbb{W}, \mathbb{V}), \end{cases} \tag{5}$$

where

$$\begin{cases} \mathbb{U}_1(t, \mathbb{X}, \mathbb{Y}, \mathbb{Z}, \mathbb{W}, \mathbb{V}) = \kappa\mathbb{Y}, \\ \mathbb{U}_2(t, \mathbb{X}, \mathbb{Y}, \mathbb{Z}, \mathbb{W}, \mathbb{V}) = \varepsilon(-\mathbb{X} - \sigma\mathbb{Y}\mathbb{Z}), \\ \mathbb{U}_3(t, \mathbb{X}, \mathbb{Y}, \mathbb{Z}, \mathbb{W}, \mathbb{V}) = \varsigma + \gamma|\mathbb{Z}| + \delta\mathbb{Y}^2, \\ \mathbb{U}_4(t, \mathbb{X}, \mathbb{Y}, \mathbb{Z}, \mathbb{W}, \mathbb{V}) \\ \qquad = -g(m + n|\mathbb{V}|)\mathbb{W} + \mathbb{Z}\mathbb{W} + e, \\ \mathbb{U}_5(t, \mathbb{X}, \mathbb{Y}, \mathbb{Z}, \mathbb{W}, \mathbb{V}) = \mathbb{W} - \mathbb{V}. \end{cases} \tag{6}$$

With the help of (6), we can express (5) as

$${}^{\mathrm{ABC}}\mathcal{D}_t^{\varpi}\psi(t) = \varrho t^{\varrho-1}A(t, \psi(t)), \quad t \in [0, T],$$
$$\psi(0) = \psi_0, \quad 0 < \varpi, \quad \varrho \leq 1$$

with the solution

$$\psi(t) = \psi_0 + \frac{\varrho(1-\varpi)t^{\varrho-1}}{\mathrm{AB}(\varpi)}A(t, \psi(t)) + \frac{\varpi\varrho}{\Gamma(\varpi)\mathrm{AB}(\varpi)}\int_0^t (t-u)^{\varpi-1}u^{\varrho-1} \times A(t, \psi(t))du, \tag{7}$$

where

$$\psi(t) = \begin{cases} \mathbb{X}(t), \\ \mathbb{Y}(t), \\ \mathbb{Z}(t), \\ \mathbb{W}(t), \\ \mathbb{V}(t), \end{cases} \quad \psi(0) = \begin{cases} \mathbb{X}(0), \\ \mathbb{Y}(0), \\ \mathbb{Z}(0), \\ \mathbb{W}(0), \\ \mathbb{V}(0), \end{cases}$$

$$A(t, \psi(t)) = \begin{cases} \mathbb{U}_1(t, \mathbb{X}, \mathbb{Y}, \mathbb{Z}, \mathbb{W}, \mathbb{V}), \\ \mathbb{U}_2(t, \mathbb{X}, \mathbb{Y}, \mathbb{Z}, \mathbb{W}, \mathbb{V}), \\ \mathbb{U}_3(t, \mathbb{X}, \mathbb{Y}, \mathbb{Z}, \mathbb{W}, \mathbb{V}), \\ \mathbb{U}_4(t, \mathbb{X}, \mathbb{Y}, \mathbb{Z}, \mathbb{W}, \mathbb{V}), \\ \mathbb{U}_5(t, \mathbb{X}, \mathbb{Y}, \mathbb{Z}, \mathbb{W}, \mathbb{V}). \end{cases}$$

Now we define a Banach space $\mathbb{B} = \mathcal{L} \times \mathcal{L} \times \mathcal{L}$ with a norm

$$\|\psi\| = \max_{t\in[0,T]} |\mathbb{X}(t) + \mathbb{Y}(t) + \mathbb{Z}(t), \mathbb{W}(t), \mathbb{V}(t)|.$$

Consider T is an operator and $T : \mathbb{B} \to \mathbb{B}$ such that

$$T(\psi(t)) = \psi_0 + \frac{\varrho(1-\varpi)t^{\varrho-1}}{\mathrm{AB}(\varpi)} A(t, \psi(t)) + \frac{\varpi\varrho}{\mathrm{AB}(\varpi)} \times \int_0^t (t-u)^{\varpi-1} u^{\varrho-1} A(t, \psi(t)) du. \quad (8)$$

Also suppose that $A(t, \psi(t))$ fulfills the Lipschitz as well as growth conditions:

- For each $\psi \in \mathbb{B}$, there exist J_A and $\mathcal{K}_A$ such that
$$|A(t, \psi(t))| \le J_A|\psi(t)| + \mathcal{K}_A. \quad (9)$$
- For every $\psi, \bar{\psi} \in \mathbb{B}$, there is $N_A > 0$ such that
$$|A(t, \psi(t)) - A(t, \bar{\psi}(t))| \le N_A|\psi(t) - \bar{\psi}(t)|. \quad (10)$$

Theorem 3. *Let us consider that* (9) *is satisfied, we also consider a function* (*continuous*) $A : [0, T] \times \mathbb{B} \to \mathcal{R}$, *so the model's solution is unique.*

Proof. Here, we show the complete continuity of T presented as (8). Since A is a continuous map, so T is also continuous. In the first part of theorem, we prove T is bounded, and second T is equi-continuous. Suppose E is a convex set $E = \{\psi \in \mathbb{B} : \|\psi\| \le \mathcal{W}, \mathcal{W} > 0\}$, for any $\psi \in \mathbb{B}$, then we have

$$\begin{aligned}
|T(\psi(t))| &= \max_{t\in[0,T]} \left|\psi_0 + \frac{\varrho(1-\varpi)t^{\varrho-1}}{\mathrm{AB}(\varpi)} A(t, \psi(t)) + \frac{\varpi\varrho}{\mathrm{AB}(\varpi)} \int_0^t (t-u)^{\varpi-1} u^{\varrho-1} A(u, \psi(u)) du\right| \\
&\le \psi_0 + \frac{\varrho(1-\varpi)T^{\varrho-1}}{\mathrm{AB}(\varpi)} (J_A|\psi(t)| + \mathcal{K}_A) + \max_{t\in[0,T]} \frac{\varpi\varrho}{\mathrm{AB}(\varpi)} \int_0^t (t-u)^{\varpi-1} u^{\varrho-1} \times |A(u, \psi(u))| du \\
&\le \psi_0 + \frac{\varrho(1-\varpi)T^{\varrho-1}}{\mathrm{AB}(\varpi)} (J_A|\psi(t)| + \mathcal{K}_A) + \frac{\varpi\varrho}{\mathrm{AB}(\varpi)\Gamma(\varpi)} (J_A|\psi(t)| + \mathcal{K}_A) T^{\varpi+\varrho-1} \times \mathbf{B}(\varpi, \varrho) \\
&\le \mathcal{W}.
\end{aligned}$$

The above result shows the boundedness of operator T.

Now, we show that T is equi-continuous. To prove this, we consider $t_1 > t_2 \in [0, T]$, so we have

$$\begin{aligned}
|T\psi(t_2) - T\psi(t_1)| &= \left|\psi_0 + \frac{\varrho(1-\varpi)t_2^{\varrho-1}}{\mathrm{AB}(\varpi)} A(t_2, \psi(t_2)) + \frac{\varpi\varrho}{\mathrm{AB}(\varpi)} \int_0^{t_2} (t_2-u)^{\varpi-1} u^{\varrho-1} \times A(u, \psi(u)) du - \psi_0 + \frac{\varrho(1-\varpi)t_1^{\varrho-1}}{\mathrm{AB}(\varpi)} \times A(t_1, \psi(t_1)) + \frac{\varpi\varrho}{\mathrm{AB}(\varpi)} \times \int_0^{t_1} (t_1-u)^{\varpi-1} u^{\varrho-1} A(u, \psi(u)) du\right| \\
&\le \frac{\varrho(1-\varpi)t_2^{\varrho-1}}{\mathrm{AB}(\varpi)} (J_A|\psi(t)| + \mathcal{K}_A) + \frac{\varpi\varrho}{\mathrm{AB}(\varpi)\Gamma(\varpi)} (J_A|\psi(t)| + \mathcal{K}_A) \times t_2^{\varpi+\varrho-1} \mathbf{B}(\varpi, \varrho) - \frac{\varrho(1-\varpi)t_1^{\varrho-1}}{\mathrm{AB}(\varpi)} \times (J_A|\psi(t)| + \mathcal{K}_A) + \frac{\varpi\varrho}{\mathrm{AB}(\varpi)\Gamma(\varpi)} \times (J_A|\psi(t)| + \mathcal{K}_A) t_1^{\varpi+\varrho-1} \mathbf{B}(\varpi, \varrho) \\
&\le \left[\frac{\varrho(1-\varpi)}{\mathrm{AB}(\varpi)} (J_A|\psi(t)| + \mathcal{K}_A)\right] \times \left(t_2^{\varrho-1} - t_1^{\varrho-1}\right) + \left[\frac{\varpi\varrho}{\mathrm{AB}(\varpi)\Gamma(\varpi)} \times (J_A|\psi(t)| + \mathcal{K}_A)\right] \times (t_2^{\varpi+\varrho-1} - t_1^{\varpi+\varrho-1}) \mathbf{B}(\varpi, \varrho).
\end{aligned}$$

Here, we examine that, when $t_1 \to t_2$, the operator $|T\psi(t_2) - T\psi(t_1)| \to 0$. Since T is continuous and bounded, so we obtain that

$$\|T\psi(t_2) - T\psi(t_1)\| \to 0 \quad \text{when } t_1 \to t_2,$$

hence it proves the operator equi-continuity of T. Hence, by using Arzela–Ascoli theorem the complete continuity of T holds. By using Schauder's theorem of fixed point result, the proposed model has a unique solution. □

Theorem 4. *Let us consider that* (10) *is satisfied, then there exists only one solution of* (7), *when*

$$\left[\frac{\varrho(1-\varpi)T^{\varrho-1}}{\mathrm{AB}(\varpi)} + \frac{\varpi\varrho}{\mathrm{AB}(\varpi)\Gamma(\varpi)}T^{\varpi-1+\varrho}\mathbf{B}(\varpi,\varrho)\right] \times N_A < 1.$$

Proof. Consider $\psi, \bar{\psi} \in \mathbb{B}$, then from (8), we have

$$\begin{aligned} |T(\psi) - T(\bar{\psi})| &= \max_{t\in[0,T]}\Bigg|\frac{\varrho(1-\varpi)t^{\varrho-1}}{\mathrm{AB}(\varpi)}(A(t,\psi(t)) - A(t,\bar{\psi}(t))) + \frac{\varpi\varrho}{\mathrm{AB}(\varpi)} \\ &\quad \times \int_0^t (t-u)^{\varpi-1}u^{\varrho-1}du(A(t,\psi(t)) - A(t,\bar{\psi}(t)))\Bigg| \\ &\le Y\|\psi - \bar{\psi}\|, \end{aligned}$$

where

$$Y = \left[\frac{\varrho(1-\varpi)T^{\varrho-1}}{\mathrm{AB}(\varpi)} + \frac{\varpi\varrho}{\mathrm{AB}(\varpi)\Gamma(\varpi)}T^{\varpi+\varrho-1}\mathbf{B}(\varpi,\varrho)\right]N_A, \quad (11)$$

which shows that T is a contraction from (10). Hence, the solution of Eq. (7) is unique. So the considered model has only one solution. □

3. DISSIPATION

The static space of system (2) is five-dimensional, hence its vector field can be defined as

$$P(A) = \begin{bmatrix} p_1(A) \\ p_2(A) \\ p_3(A) \\ p_4(A) \\ p_5(A) \end{bmatrix} = \begin{bmatrix} \kappa\mathbb{Y} \\ \varepsilon(-\mathbb{X} - \sigma\mathbb{Y}\mathbb{Z}) \\ \varsigma + \gamma|\mathbb{Z}| + \delta\mathbb{Y}^2 \\ -g(m+n|\mathbb{V}|)\mathbb{W} + \mathbb{Z}\mathbb{W} + e \\ \mathbb{W} - \mathbb{V} \end{bmatrix}. \quad (12)$$

From the vector field presented above, the divergence can be obtained as

$$\begin{aligned} \nabla V &= \epsilon\sigma\mathbb{Z} + \gamma\frac{\mathbb{Z}}{|\mathbb{Z}|} - g(m+n|\mathbb{V}|) + \mathbb{Z} - 1 \\ &= \mathbb{Z}\left(\epsilon\sigma + \gamma\frac{1}{|\mathbb{Z}|} + 1\right) - (g(m+n|\mathbb{V}|) + 1), \end{aligned} \quad (13)$$

where $\nabla V = p_{1\mathbb{X}} + p_{2\mathbb{Y}} + p_{3\mathbb{Z}} + p_{4\mathbb{W}} + p_{5\mathbb{V}}$. From Eq. (1), it can be seen that system (13) is of dissipative nature as long as $g > 0$ which makes $\nabla V < 0$. Also, we observe that model (1) converges in the exponential form $\frac{dV}{dt} = \exp(-\{\mathbb{Z}(\epsilon\sigma + \gamma\frac{1}{|\mathbb{Z}|} + 1) - (g(m + n|\mathbb{V}|) + 1)\}t)$. When $t \to \infty$, all the trajectories of the model will eventually be constrained to a set having zero volume, due to this the extreme motion will converge to an attractor. This proves that there exists an attractor in the suggested system (1).

4. POINCARÉ MAPS

The Poincaré map is an important technique, which analyzes the folding properties and bifurcation of chaos in a dynamical system. Here we take

$$\begin{cases} \sum_1 = [\mathbb{X},\mathbb{Y},\mathbb{Z},\mathbb{W},\mathbb{V}]^{\mathfrak{T}} \in R^3|\mathbb{X} = 1, \\ \sum_2 = [\mathbb{X},\mathbb{Y},\mathbb{Z},\mathbb{W},\mathbb{V}]^{\mathfrak{T}} \in R^3|\mathbb{Y} = 1, \\ \sum_3 = [\mathbb{X},\mathbb{Y},\mathbb{Z},\mathbb{W},\mathbb{V}]^{\mathfrak{T}} \in R^3|\mathbb{Z} = 1, \\ \sum_3 = [\mathbb{X},\mathbb{Y},\mathbb{Z},\mathbb{W},\mathbb{V}]^{\mathfrak{T}} \in R^3|\mathbb{W} = 1, \\ \sum_3 = [\mathbb{X},\mathbb{Y},\mathbb{Z},\mathbb{W},\mathbb{V}]^{\mathfrak{T}} \in R^3|\mathbb{V} = 1 \end{cases} \quad (14)$$

as cross sections.

In order to analyze the Poincaré sections for system (2), we choose the parameter values to be $\kappa = \varepsilon = 1.01$, $\sigma = -1$, $\varsigma = 2$, $\gamma = m = n = 1$, $\delta = -1$, and $g = e = 20$. First, we present the effects of fractional order on the model dynamics by fixing the fractal dimension which is considered to be $\varrho = 0.98$ and for a variety of fractional orders. In Figs. 1a–1d, the fractional orders for the different colors are considered as: 0.99 (blue), 0.98 (red), 0.95 (green), and 0.94 (black). These figures show that at lower fractional orders the system is evolving into a symmetric limit-cycle attractor. Figures 2a–2b show the effects of varying fractal dimension ϱ on the

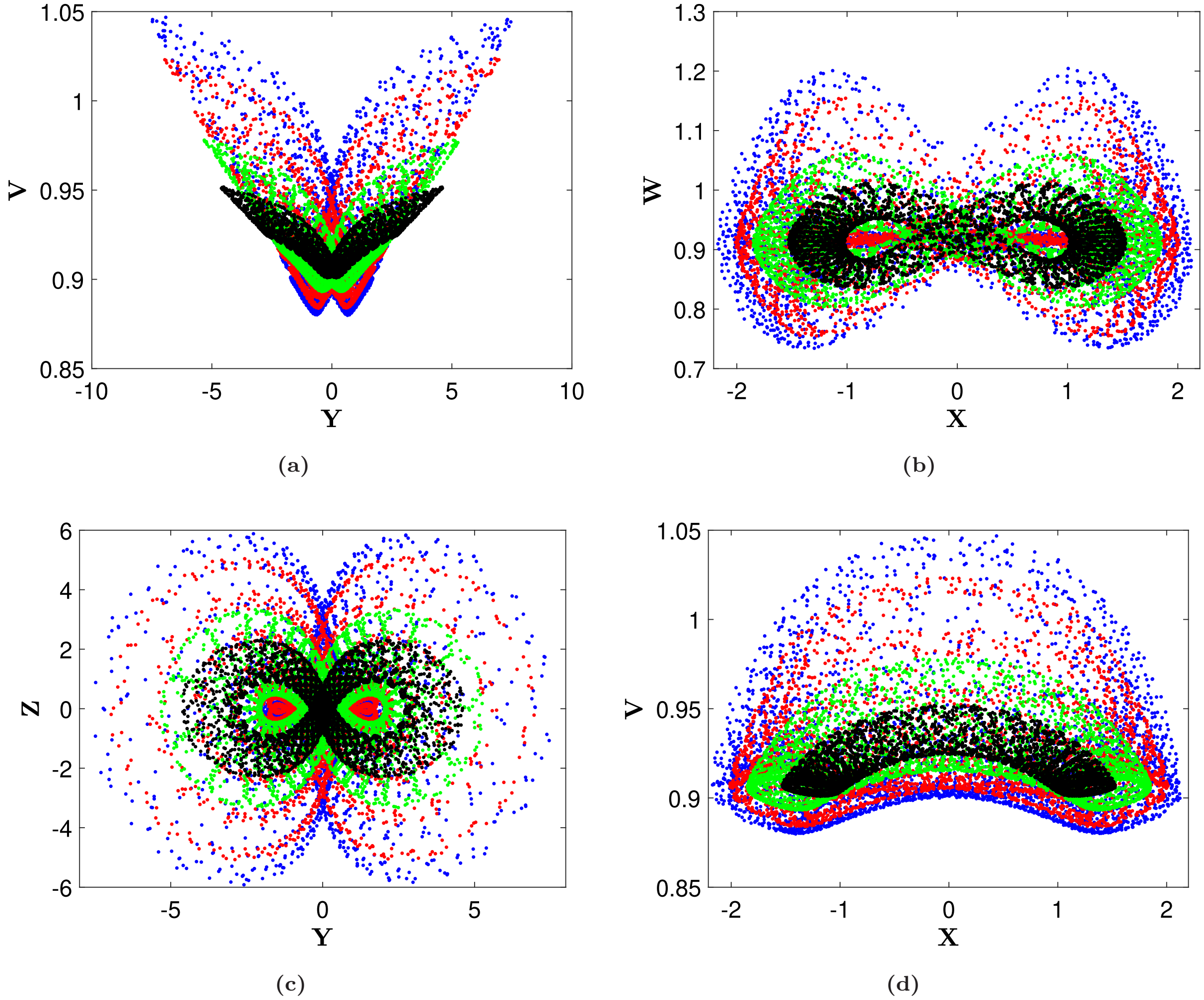

Fig. 1 The Poincaré sections of different state variables of system (2) with varying fractional order ϖ and fixed fractal dimension $\varrho = 0.98$.

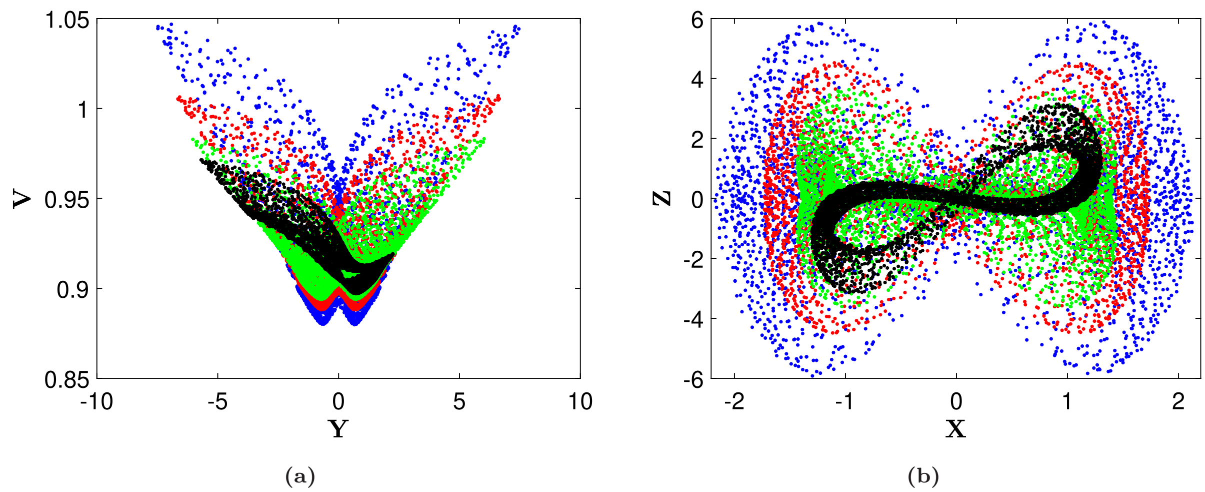

Fig. 2 The Poincaré sections of different state variables of system (2) with varying fractal dimension ϖ and fixed fractional order ϱ.

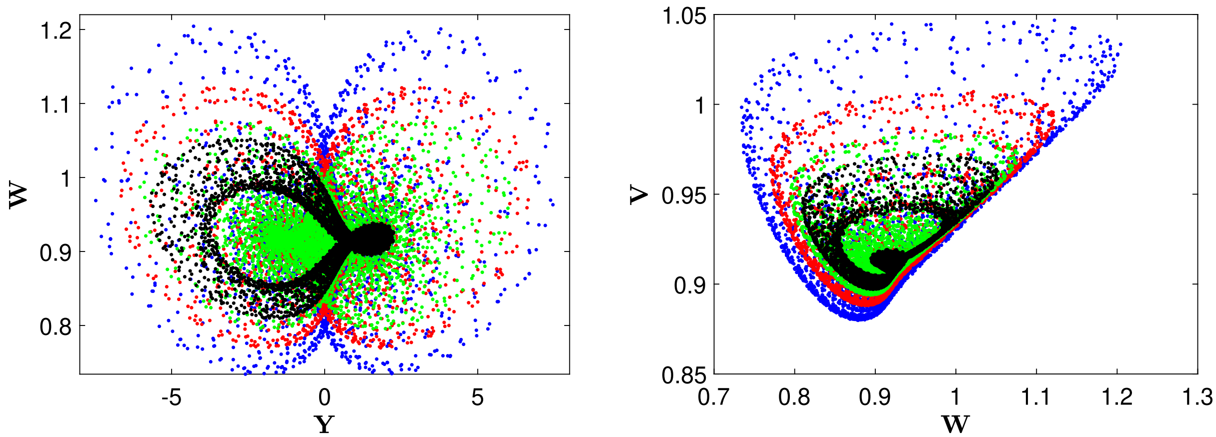

(c) (d)

Fig. 2 (*Continued*)

dynamics of system (2) with fixed $\varpi = 0.98$. The values of ϱ for different colors are taken to be: 0.98 (blue), 0.97 (red), 0.96 (green), and 0.95 (black). Lowering the value of the fractal dimension, we see the emergence of the asymmetric attractor in the suggested system (2). It can also be observed that branches are integrated, which in turn connect as a single attractor in the Poincaré section.

5. NUMERICAL SCHEME FOR DOUBLING MEMRISTORS MODEL

Here, we approximate the solution of the system numerically with Newton's Polynomial Interpolation scheme,[31]

$$\begin{cases} {}_0^{\mathrm{FFM}}\mathbf{D}_t^{\varpi,\varrho}\mathbb{X}(t) = \kappa\mathbb{Y}, \\ {}_0^{\mathrm{FFM}}\mathbf{D}_t^{\varpi,\varrho}\mathbb{Y}(t) = \varepsilon(-\mathbb{X} - \sigma\mathbb{Y}\mathbb{Z}), \\ {}_0^{\mathrm{FFM}}\mathbf{D}_t^{\varpi,\varrho}\mathbb{Z}(t) = \varsigma + \gamma|\mathbb{Z}| + \delta\mathbb{Y}^2, \\ {}_0^{\mathrm{FFM}}\mathbf{D}_t^{\varpi,\varrho}\mathbb{W}(t) = -g(m + n|\mathbb{V}|)\mathbb{W} + \mathbb{Z}\mathbb{W} + e, \\ {}_0^{\mathrm{FFM}}\mathbf{D}_t^{\varpi,\varrho}\mathbb{V}(t) = \mathbb{W} - \mathbb{V}. \end{cases} \tag{15}$$

Using integration and doing some manipulation, we get

$$\begin{aligned} \mathbb{X}^{k+1} &= \mathbb{X}_0 + \frac{1-\nu}{\mathrm{AB}(\nu)}\varpi t_k^{\varpi-1} h_1(t_k, \mathbb{X}^k, \mathbb{Y}^k, \mathbb{Z}^k, \\ &\quad \mathbb{W}^k, \mathbb{V}^k) + \frac{\nu(\Delta t)^\nu}{\mathrm{AB}(\nu)\Gamma(\nu+1)} \\ &\quad \times \sum_{p=2}^{k} \varpi t_{p-2}^{\varpi-1} h_1(t_{p-2}, \mathbb{X}^{p-2}, \mathbb{Y}^{p-2}, \\ &\quad \mathbb{Z}^{p-2}, \mathbb{W}^{p-2}, \mathbb{V}^{p-2}) \\ &\quad \times [(k-p+1)^\nu - (k-p)^\nu] \\ &\quad + \frac{\nu(\Delta t)^\nu}{\mathrm{AB}(\nu)\Gamma(\nu+2)} \\ &\quad \times \sum_{p=2}^{k} \begin{bmatrix} \varpi t_{p-1}^{\varpi-1} h_1(t_{p-1}, \mathbb{X}^{p-1}, \mathbb{Y}^{p-1}, \\ \mathbb{Z}^{p-1}, \mathbb{W}^{p-1}, \mathbb{V}^{p-1}) \\ -\varpi t_{p-2}^{\varpi-1} h_1(t_{p-2}, \mathbb{X}^{p-2}, \mathbb{Y}^{p-2}, \\ \mathbb{Z}^{p-2}, \mathbb{W}^{p-2}, \mathbb{V}^{p-2}) \end{bmatrix} \\ &\quad \times \begin{bmatrix} (k-p+1)^\nu (k-p+3+2\nu) \\ -(k-p+1)^\nu (k-p+3+3\nu)^\nu \end{bmatrix} \\ &\quad + \frac{\nu(\Delta t)^\nu}{2\mathrm{AB}(\nu)\Gamma(\nu+3)} \\ &\quad \times \sum_{p=2}^{k} \begin{bmatrix} \varpi t_p^{\varpi-1} h_1(t_p, \mathbb{X}^p, \mathbb{Y}^p, \mathbb{Z}^p, \mathbb{W}^p, \mathbb{V}^p) \\ -2\varpi t_{p-1}^{\varpi-1} h_1(t_{p-1}, \mathbb{X}^{p-1}, \mathbb{Y}^{p-1}, \\ \mathbb{Z}^{p-1}, \mathbb{W}^{p-1}, \mathbb{V}^{p-1}) \\ +\varpi t_{p-2}^{\varpi-1} h_1(t_{p-2}, \mathbb{X}^{p-2}, \mathbb{Y}^{p-2}, \\ \mathbb{Z}^{p-2}, \mathbb{W}^{p-2}, \mathbb{V}^{p-2}) \end{bmatrix} \\ &\quad \times \begin{bmatrix} (k-p+1)^\nu [2(k-p)^2 + (3\nu+10) \\ \times (k-p) + 2\nu^2 + 9\nu + 12] \\ -(k-p)^\nu [2(k-p)^2 + (5\nu+10) \\ \times (k-p) + 6\nu^2 + 18\nu + 12] \end{bmatrix}, \end{aligned} \tag{16}$$

$$\begin{aligned}\mathbb{Y}^{k+1} &= \mathbb{Y}_0 + \frac{1-\nu}{\mathrm{AB}(\nu)}\varpi t_k^{\varpi-1} h_3(t_k, \mathbb{X}^k, \mathbb{Y}^k, \mathbb{Z}^k, \\ &\quad \mathbb{W}^k, \mathbb{V}^k) + \frac{\nu(\Delta t)^\nu}{\mathrm{AB}(\nu)\Gamma(\nu+1)} \\ &\quad \times \sum_{p=2}^{k} \varpi t_{p-2}^{\varpi-1} h_3(t_{p-2}, \mathbb{X}^{p-2}, \mathbb{Y}^{p-2}, \\ &\quad \mathbb{Z}^{p-2}, \mathbb{W}^{p-2}, \mathbb{V}^{p-2}) \\ &\quad \times [(k-p+1)^\nu - (k-p)^\nu] \\ &\quad + \frac{\nu(\Delta t)^\nu}{\mathrm{AB}(\nu)\Gamma(\nu+2)} \\ &\quad \times \sum_{p=2}^{k} \begin{bmatrix} \varpi t_{p-1}^{\varpi-1} h_3(t_{p-1}, \mathbb{X}^{p-1}, \mathbb{Y}^{p-1}, \\ \mathbb{Z}^{p-1}, \mathbb{W}^{p-1}, \mathbb{V}^{p-1}) \\ -\varpi t_{p-2}^{\varpi-1} h_3(t_{p-2}, \mathbb{X}^{p-2}, \mathbb{Y}^{p-2}, \\ \mathbb{Z}^{p-2}, \mathbb{W}^{p-2}, \mathbb{V}^{p-2}) \end{bmatrix} \\ &\quad \times \begin{bmatrix} (k-p+1)^\nu (k-p+3+2\nu) \\ -(k-p+1)^\nu (k-p+3+3\nu)^\nu \end{bmatrix} \\ &\quad + \frac{\nu(\Delta t)^\nu}{2\mathrm{AB}(\nu)\Gamma(\nu+3)} \\ &\quad \times \sum_{p=2}^{k} \begin{bmatrix} \varpi t_p^{\varpi-1} h_3(t_p, \mathbb{X}^p, \mathbb{Y}^p, \mathbb{Z}^p, \mathbb{W}^p, \mathbb{V}^p) \\ -2\varpi t_{p-1}^{\varpi-1} h_3(t_{p-1}, \mathbb{X}^{p-1}, \mathbb{Y}^{p-1}, \\ \mathbb{Z}^{p-1}, \mathbb{W}^{p-1}, \mathbb{V}^{p-1}) \\ +\varpi t_{p-2}^{\varpi-1} (t_{p-2}, \mathbb{X}^{p-2}, \mathbb{Y}^{p-2}, \\ \mathbb{Z}^{p-2}, \mathbb{W}^{p-2}, \mathbb{V}^{p-2}) \end{bmatrix} \\ &\quad \times \begin{bmatrix} (k-p+1)^\nu [2(k-p)^2 + (3\nu+10) \\ \times (k-p) + 2\nu^2 + 9\nu + 12] \\ -(k-p)^\nu [2(k-p)^2 + (5\nu+10) \\ \times (k-p) + 6\nu^2 + 18\nu + 12] \end{bmatrix}, \end{aligned} \tag{17}$$

$$\begin{aligned}\mathbb{Z}^{k+1} &= \mathbb{Z}_0 + \frac{1-\nu}{\mathrm{AB}(\nu)}\varpi t_k^{\varpi-1} h_3(t_k, \mathbb{X}^k, \mathbb{Y}^k, \\ &\quad \mathbb{Z}^k, \mathbb{W}^k, \mathbb{V}^k) + \frac{\nu(\Delta t)^\nu}{\mathrm{AB}(\nu)\Gamma(\nu+1)} \\ &\quad \times \sum_{p=2}^{k} \varpi t_{p-2}^{\varpi-1} h_3(t_{p-2}, \mathbb{X}^{p-2}, \mathbb{Y}^{p-2}, \mathbb{Z}^{p-2}, \\ &\quad \mathbb{W}^{p-2}, \mathbb{V}^{p-2})[(k-p+1)^\nu - (k-p)^\nu] \\ &\quad + \frac{\nu(\Delta t)^\nu}{\mathrm{AB}(\nu)\Gamma(\nu+2)} \\ &\quad \times \sum_{p=2}^{k} \begin{bmatrix} \varpi t_{p-1}^{\varpi-1} h_3(t_{p-1}, \mathbb{X}^{p-1}, \mathbb{Y}^{p-1}, \\ \mathbb{Z}^{p-1}, \mathbb{W}^{p-1}, \mathbb{V}^{p-1}) \\ -\varpi t_{p-2}^{\varpi-1} h_3(t_{p-2}, \mathbb{X}^{p-2}, \mathbb{Y}^{p-2}, \\ \mathbb{Z}^{p-2}, \mathbb{W}^{p-2}, \mathbb{V}^{p-2}) \end{bmatrix} \\ &\quad \times \begin{bmatrix} (k-p+1)^\nu (k-p+3+2\nu) \\ -(k-p+1)^\nu (k-p+3+3\nu)^\nu \end{bmatrix} \\ &\quad + \frac{\nu(\Delta t)^\nu}{2\mathrm{AB}(\nu)\Gamma(\nu+3)} \\ &\quad \times \sum_{p=2}^{k} \begin{bmatrix} \varpi t_p^{\varpi-1} h_3(t_p, \mathbb{X}^p, \mathbb{Y}^p, \mathbb{Z}^p, \mathbb{W}^p, \mathbb{V}^p) \\ -2\varpi t_{p-1}^{\varpi-1} h_3(t_{p-1}, \mathbb{X}^{p-1}, \mathbb{Y}^{p-1}, \\ \mathbb{Z}^{p-1}, \mathbb{W}^{p-1}, \mathbb{V}^{p-1}) \\ +\varpi t_{p-2}^{\varpi-1} h_3(t_{p-2}, \mathbb{X}^{p-2}, \mathbb{Y}^{p-2}, \\ \mathbb{Z}^{p-2}, \mathbb{W}^{p-2}, \mathbb{V}^{p-2}) \end{bmatrix} \\ &\quad \times \begin{bmatrix} (k-p+1)^\nu [2(k-p)^2 + (3\nu+10) \\ \times (k-p) + 2\nu^2 + 9\nu + 12] \\ -(k-p)^\nu [2(k-p)^2 + (5\nu+10) \\ \times (k-p) + 6\nu^2 + 18\nu + 12] \end{bmatrix}, \end{aligned} \tag{18}$$

$$\begin{aligned}\mathbb{W}^{k+1} &= \mathbb{W}_0 + \frac{1-\nu}{\mathrm{AB}(\nu)}\varpi t_k^{\varpi-1} h_4(t_k, \mathbb{X}^k, \mathbb{Y}^k, \\ &\quad \mathbb{Z}^k, \mathbb{W}^k, \mathbb{V}^k) + \frac{\nu(\Delta t)^\nu}{\mathrm{AB}(\nu)\Gamma(\nu+1)} \\ &\quad \times \sum_{p=2}^{k} \varpi t_{p-2}^{\varpi-1} h_4(t_{p-2}, \mathbb{X}^{p-2}, \mathbb{Y}^{p-2}, \\ &\quad \mathbb{Z}^{p-2}, \mathbb{W}^{p-2}, \mathbb{V}^{p-2}) \\ &\quad \times [(k-p+1)^\nu - (k-p)^\nu] \\ &\quad + \frac{\nu(\Delta t)^\nu}{\mathrm{AB}(\nu)\Gamma(\nu+2)} \\ &\quad \times \sum_{p=2}^{k} \begin{bmatrix} \varpi t_{p-1}^{\varpi-1} h_4(t_{p-1}, \mathbb{X}^{p-1}, \mathbb{Y}^{p-1}, \\ \mathbb{Z}^{p-1}, \mathbb{W}^{p-1}, \mathbb{V}^{p-1}) \\ -\varpi t_{p-2}^{\varpi-1} h_4(t_{p-2}, \mathbb{X}^{p-2}, \mathbb{Y}^{p-2}, \\ \mathbb{Z}^{p-2}, \mathbb{W}^{p-2}, \mathbb{V}^{p-2}) \end{bmatrix} \\ &\quad \times \begin{bmatrix} (k-p+1)^\nu (k-p+3+2\nu) \\ -(k-p+1)^\nu (k-p+3+3\nu)^\nu \end{bmatrix} \\ &\quad + \frac{\nu(\Delta t)^\nu}{2\mathrm{AB}(\nu)\Gamma(\nu+3)} \end{aligned}$$

$$\times \sum_{p=2}^{k} \begin{bmatrix} \varpi t_p^{\varpi-1} h_4(t_p, \mathbb{X}^p, \mathbb{Y}^p, \mathbb{Z}^p, \mathbb{W}^p, \mathbb{V}^p) \\ -2\varpi t_{p-1}^{\varpi-1} h_3(t_{p-1}, \mathbb{X}^{p-1}, \mathbb{Y}^{p-1}, \\ \mathbb{Z}^{p-1}, \mathbb{W}^{p-1}, \mathbb{V}^{p-1}) \\ +\varpi t_{p-2}^{\varpi-1} h_3(t_{p-2}, \mathbb{X}^{p-2}, \mathbb{Y}^{p-2}, \\ \mathbb{Z}^{p-2}, \mathbb{W}^{p-2}, \mathbb{V}^{p-2}) \end{bmatrix} \times \begin{bmatrix} (k-p+1)^\nu [2(k-p)^2 + (3\nu+10) \\ \times (k-p) + 2\nu^2 + 9\nu + 12] \\ -(k-p)^\nu [2(k-p)^2 + (5\nu+10) \\ \times (k-p) + 6\nu^2 + 18\nu + 12] \end{bmatrix}, \tag{19}$$

$$\begin{aligned} \mathbb{V}^{k+1} = {} & \mathbb{V}_0 + \frac{1-\nu}{\mathrm{AB}(\nu)} \varpi t_k^{\varpi-1} h_5 \\ & \times (t_k, \mathbb{X}^k, \mathbb{Y}^k, \mathbb{Z}^k, \mathbb{W}^k, \mathbb{V}^k) \\ & + \frac{\nu(\Delta t)^\nu}{\mathrm{AB}(\nu)\Gamma(\nu+1)} \sum_{p=2}^{k} \varpi t_{p-2}^{\varpi-1} h_5 \\ & \times (t_{p-2}, \mathbb{X}^{p-2}, \mathbb{Y}^{p-2}, \mathbb{Z}^{p-2}, \mathbb{W}^{p-2}, \mathbb{V}^{p-2}) \\ & \times [(k-p+1)^\nu - (k-p)^\nu] \\ & + \frac{\nu(\Delta t)^\nu}{\mathrm{AB}(\nu)\Gamma(\nu+2)} \\ & \times \sum_{p=2}^{k} \begin{bmatrix} \varpi t_{p-1}^{\varpi-1} h_5(t_{p-1}, \mathbb{X}^{p-1}, \mathbb{Y}^{p-1}, \mathbb{Z}^{p-1}, \\ \mathbb{W}^{p-1}, \mathbb{V}^{p-1}) \\ -\varpi t_{p-2}^{\varpi-1} h_5(t_{p-2}, \mathbb{X}^{p-2}, \mathbb{Y}^{p-2}, \\ \mathbb{Z}^{p-2}, \mathbb{W}^{p-2}, \mathbb{V}^{p-2}) \end{bmatrix} \\ & \times \begin{bmatrix} (k-p+1)^\nu (k-p+3+2\nu) \\ -(k-p+1)^\nu (k-p+3+3\nu)^\nu \end{bmatrix} \\ & + \frac{\nu(\Delta t)^\nu}{2\mathrm{AB}(\nu)\Gamma(\nu+3)} \\ & \times \sum_{p=2}^{k} \begin{bmatrix} \varpi t_p^{\varpi-1} h_5(t_p, \mathbb{X}^p, \mathbb{Y}^p, \mathbb{Z}^p, \mathbb{W}^p, \mathbb{V}^p) \\ -2\varpi t_{p-1}^{\varpi-1} h_5(t_{p-1}, \mathbb{X}^{p-1}, \mathbb{Y}^{p-1}, \\ \mathbb{Z}^{p-1}, \mathbb{W}^{p-1}, \mathbb{V}^{p-1}) \\ +\varpi t_{p-2}^{\varpi-1} h_3(t_{p-2}, \mathbb{X}^{p-2}, \mathbb{Y}^{p-2}, \\ \mathbb{Z}^{p-2}, \mathbb{W}^{p-2}, \mathbb{V}^{p-2}) \end{bmatrix} \\ & \times \begin{bmatrix} (k-p+1)^\nu [2(k-p)^2 \\ +(3\nu+10)(k-p) + 2\nu^2 \\ +9\nu + 12] - (k-p)^\nu [2(k-p)^2 \\ +(5\nu+10)(k-p) + 6\nu^2 \\ +18\nu + 12] \end{bmatrix}, \end{aligned} \tag{20}$$

where

$$\begin{aligned} & h_1(t_q, \mathbb{X}^q, \mathbb{Y}^q, \mathbb{Z}^q, \mathbb{W}^q, \mathbb{V}^q) = \kappa \mathbb{Y}^q, \\ & h_2(t_q, \mathbb{X}^q, \mathbb{Y}^q, \mathbb{Z}^q, \mathbb{W}^q, \mathbb{V}^q) = \varepsilon(-\mathbb{X}^q - \sigma \mathbb{Y}^q \mathbb{Z}^q), \\ & h_3(t_q, \mathbb{X}^q, \mathbb{Y}^q, \mathbb{Z}^q, \mathbb{W}^q, \mathbb{V}^q) \\ & \qquad = \varsigma + \gamma|\mathbb{Z}| + \delta \mathbb{Y}^{2p}, \\ & h_4(t_q, \mathbb{X}^q, \mathbb{Y}^q, \mathbb{Z}^q, \mathbb{W}^q, \mathbb{V}^q) \\ & \qquad = -g(m + n|\mathbb{V}^q|)\mathbb{W}^q + \mathbb{Z}^q \mathbb{W}^q + e, \\ & h_5(t_q, \mathbb{X}^q, \mathbb{Y}^q, \mathbb{Z}^q, \mathbb{W}^q, \mathbb{V}^q) = \mathbb{W}^q - \mathbb{V}^q, \end{aligned} \tag{21}$$

where $q = p$, $p-1$, and $p-2$, respectively.

6. NUMERICAL SIMULATIONS AND DISCUSSION ON FINDINGS

This section provides a detailed analysis of the double memristor model (2) with ranges of different fractional orders ϖ and fractal dimensions ϱ. The evolution, projection, and emergence of different attractors are observed with different values of ϖ and ϱ. In the simulation of the numerical approximation of system (2), we have considered the time $t = 200$ with a step size $h = 0.001$ making the number of iterations to be 2×10^5. The parameter values considered for the numerical illustrations are $\kappa = \varepsilon = 1.01, \sigma = -1, \varsigma = 2, \gamma = m = n = 1, \delta = -1$, and $g = e = 20$, and the initial values are used as $[\mathbb{X}, \mathbb{Y}, \mathbb{Z}, \mathbb{W}, \mathbb{V}] = [1, -1, 2, 1, 1]$.

First, we are interested to observe and understand how the system dynamically changes with variations in the fractional order while keeping the fractal dimension constant. So, we present the dynamics in different state variables' phase planes. From Figs. 3–7, the evolutions of the attractors in the proposed system are demonstrated with ϱ to be 1, 0.98, 0.96, 0.94, and 0.90, respectively. In Figs. 3a, 4b, 5b, 6b, and 7a the projections in $\mathbb{Y}$–$\mathbb{V}$-plane are presented. In Figs. 3c, 4c, 5c, 6c, and 7b, the dynamics in $\mathbb{X}$–$\mathbb{W}$-plane is projected. Similarly, in Figs. 3c, 4c, 5c, 6c, 7c and 3d, 4d, 5d, 6d, 7d, the dynamics in $\mathbb{Y}$–$\mathbb{Z}$- and $\mathbb{Z}$–$\mathbb{W}$-planes are depicted, respectively. Moreover, in Figs. 3e, 4e, 5e, 6e, 7e and 3f, 4f, 5f, 6f, 7f, the 3D behaviors of the system's phase planes t–$\mathbb{Y}$–$\mathbb{Z}$ and t–$\mathbb{Y}$–$\mathbb{Z}$, respectively, are depicted. In Fig. 3a, it is observed that the numerical technique used above for the numerical approximations is quickly convergent, showing

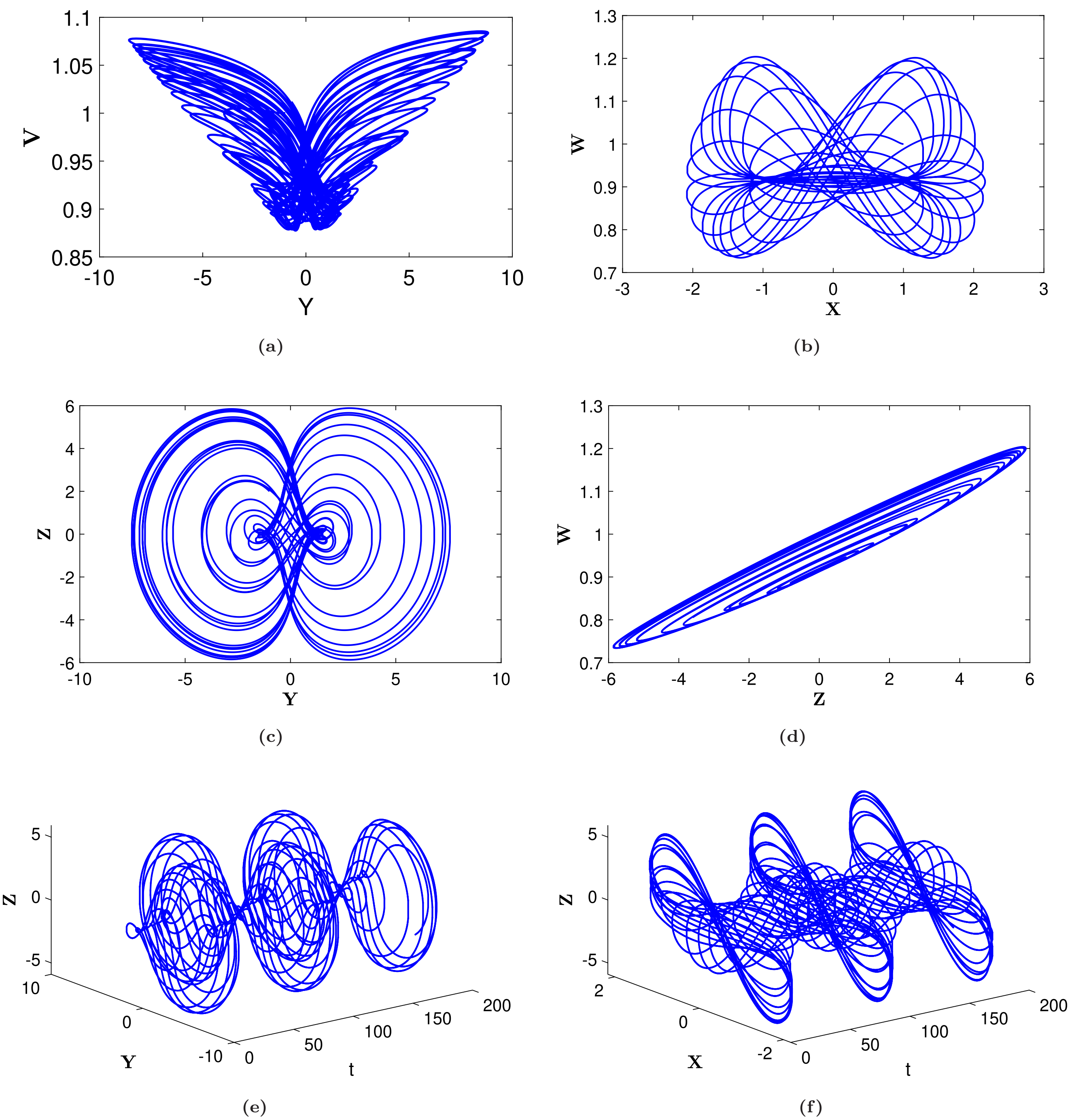

Fig. 3 The behaviors of different state variables of system (2) with fractional order $\varpi = 1$ and fixed fractal dimension $\varrho = 1$.

the dynamics of the system as observed with the integer-order derivative, here $\varpi = \varrho = 1$. Now at $\varpi = 0.98$, one can see that the emergence of limit-cycle attractor has occurred in Fig. 4. Further decreasing ϖ to 0.96, the system converges to the attractor more rapidly as compared to $\varpi = 0.98$, i.e. at $t = 50$ it can be seen that the attractor appears and the trajectories evolve toward it. At $\varpi = 0.96$ and $\varpi = 0.94$, the system seems to reduce its complex nature and converge to the attractor at $t = 30$ and $t = 20$, respectively. Finally at $\varpi = 0.90$, it is observed that the system converges to the attractors as soon as $t = 10$ with regular oscillations of same amplitudes, showing that the system is

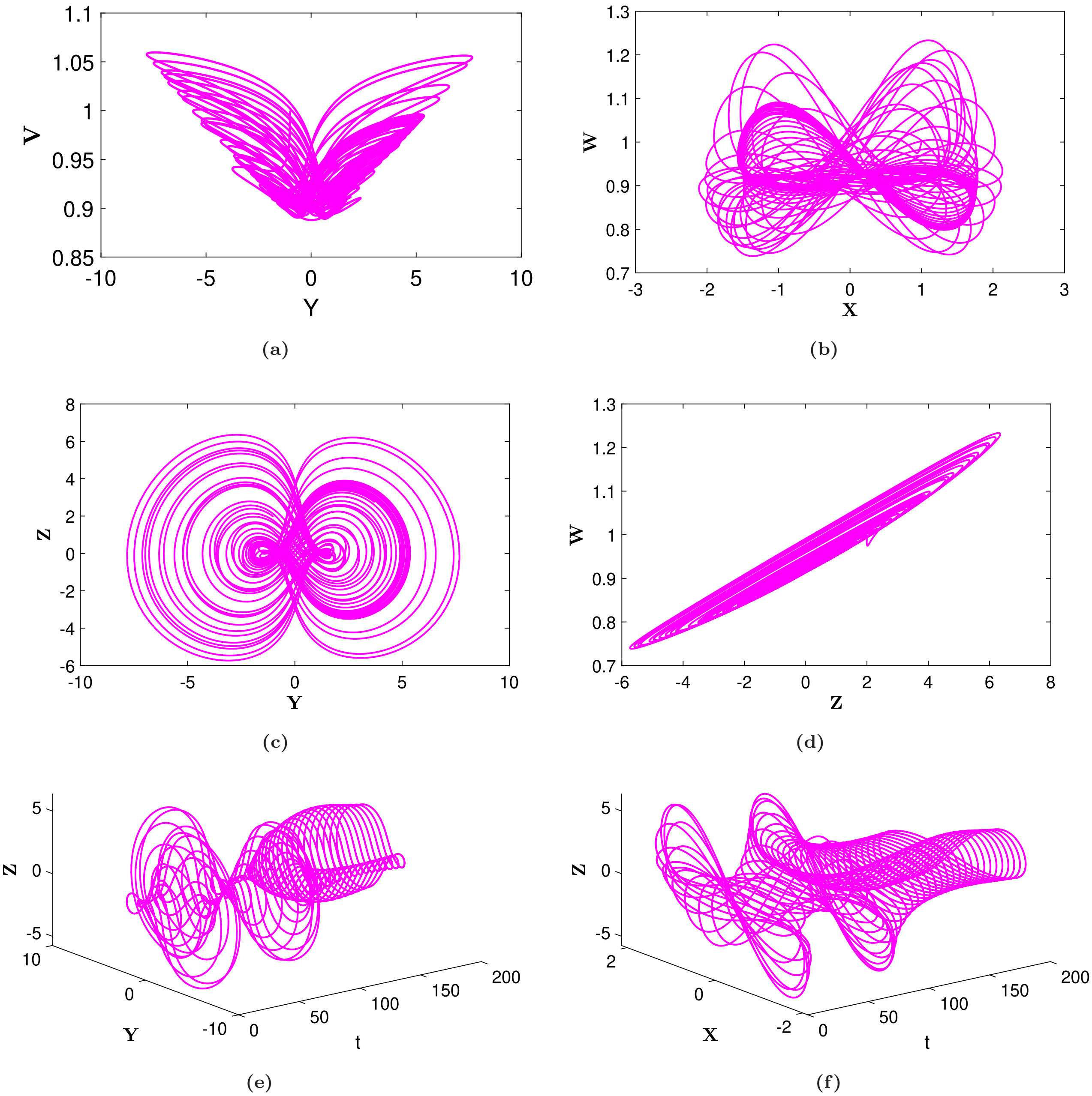

Fig. 4 The behaviors of different state variables of system (2) with $\varrho = 0.98$ and fixed fractal dimension ϖ.

dynamically restricted to a specific region due to which one can predict about the existence of a point at some t. Overall, we observe that the fractional order shows a significant impact on the dynamics which reduces the extreme complex nature of the suggested double memristor model (2) to a more simpler one by decreasing the amplitudes of oscillations and restricting the trajectories toward a limit-cycle attractor.

In Figs. 8a–8f, the dynamics of the system is illustrated with fixed $\varpi = 0.98$ and different fractal dimensions. The colors used in these figures represent the dimensions as: blue: 0.99, magenta: 0.98, green: 0.97, red: 0.96, and black = 0.95. Figure 8a shows the effects of different fractal dimensions on the system's phase plane $\mathbb{X}$–$\mathbb{Z}$. Figure 8c demonstrates the effects of various values of ϱ in the $\mathbb{Y}$–$\mathbb{Z}$-plane. Similarly, Figs. 8d–8f depict the nature of

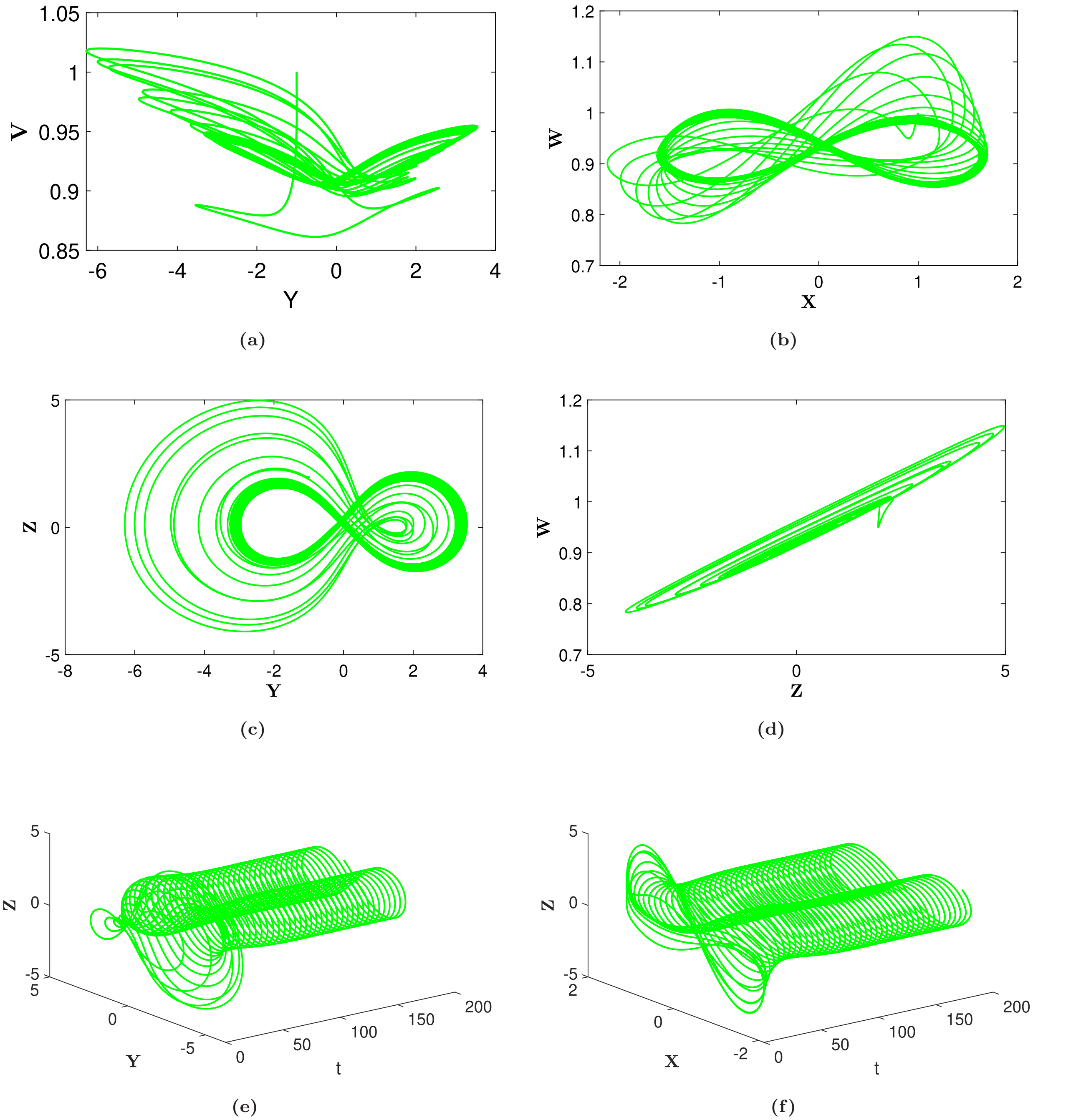

Fig. 5 The behaviors of different state variables of system (2) with $\varrho = 0.96$ and fixed fractal dimension ϖ.

the dynamical variations in the planes $\mathbb{Y}$–$\mathbb{W}$, t–$\mathbb{Y}$–$\mathbb{Z}$, and t–$\mathbb{X}$–$\mathbb{Z}$, respectively.

Further, Figs. 9a–9e show the oscillations versus time t in the system classes $\mathbb{X}$, $\mathbb{Y}$, $\mathbb{Z}$, $\mathbb{W}$, and $\mathbb{V}$, respectively, with different fractional orders. In Fig. 9a, one can observe that at lower order the system is oscillating with the same amplitudes which makes the system to converge to an attractor. Furthermore, in other classes it is also observed that the system is evolving toward an attractor and the random oscillations are no more present in the system with lower fractional orders.

Figures 10a–10e show the dynamics versus time t in the system states $\mathbb{X}$, $\mathbb{Y}$, $\mathbb{Z}$, $\mathbb{W}$, and $\mathbb{V}$, respectively,

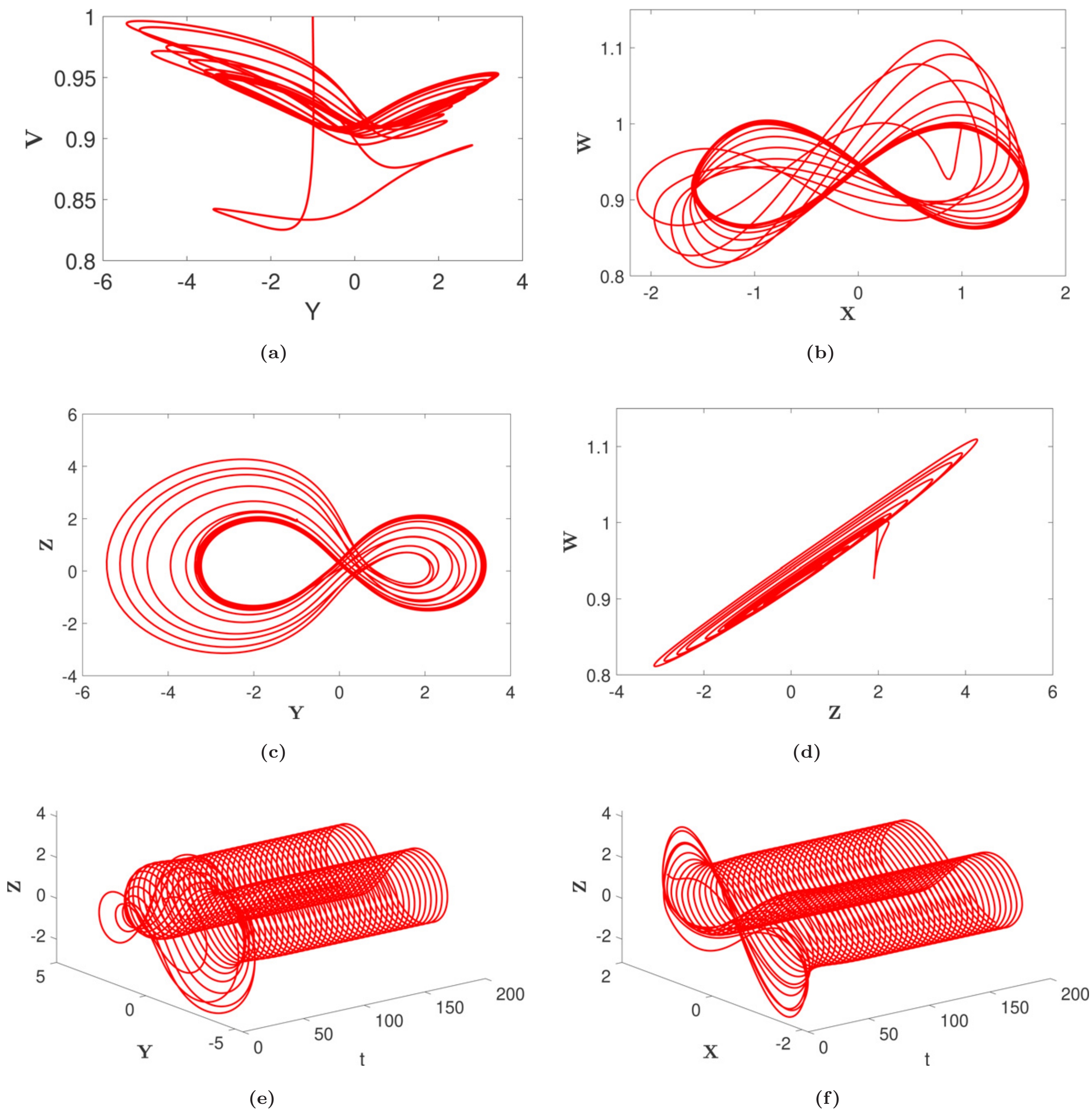

Fig. 6 The behaviors of different state variables of system (2) with $\varrho = 0.94$ and fixed fractal dimension ϖ.

with various values of fractal dimension. Here, we see that the number of oscillations is more as compared to that with varying ϖ. From the variations in ϱ, it is observed that when we decrease the fractal dimension self-similar pattern is observed together with a decrease in the amplitudes of the oscillations of different classes.

Figure 11 shows the sensitive dependence of different state variables of model (2), where the red-colored curves represent the dynamics with the initial values $[\mathbb{X}, \mathbb{Y}, \mathbb{Z}, \mathbb{W}, \mathbb{V}] = [1, -1.4, 2, 1, 1]$ and the black-colored curves present the dynamics with initial values $[\mathbb{X}, \mathbb{Y}, \mathbb{Z}, \mathbb{W}, \mathbb{V}] = [1, -1, 2, 1, 1]$. Further, Fig. 11a shows the sensitivity of the state variable $\mathbb{X}$ toward the initial values. Similarly, Figs. 11b and 11c are provided to observe the evolutions in the dynamics of system's state variables $\mathbb{Y}$ and $\mathbb{Z}$, respectively. Finally, Figs. 11d and 11e show the dynamics of system's state variables $\mathbb{Y}$ and $\mathbb{Z}$ versus time t with different initial conditions. We observed

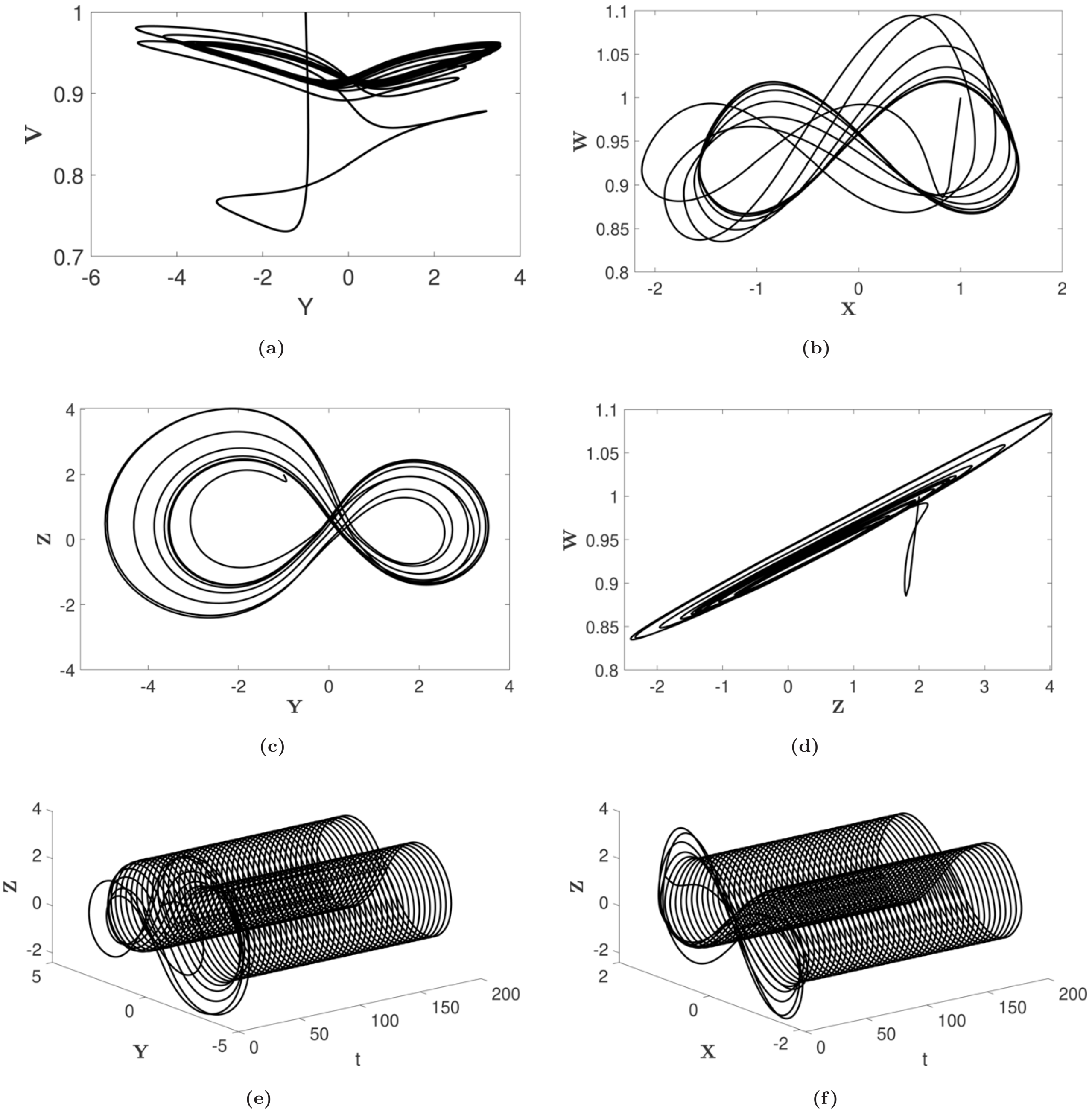

Fig. 7 The behaviors of different state variables of system (2) with $\varrho = 0.90$ and fixed fractal dimension ϖ.

that even a slight change in the initial values produces great change in the behavior of the system, which shows the chaotic nature of the considered system.

Remark 5. The robustness and novelty of the proposed approach are discussed in Fig. 12. Figures 12a and 12b show the dynamics of $\mathcal{Z}$–$\mathcal{X}$ and $\mathcal{Z}$–$\mathcal{Y}$ classes for integer and fractional orders of 0.92, respectively. Similarly, Figs. 12c and 12d portray the behaviors of $\mathcal{Z}$–$\mathcal{X}$ and $\mathcal{Z}$–$\mathcal{Y}$ classes for integer and fractal orders of 0.9, respectively. From these simulations, we conclude that the considered model (2) gives the hidden chaotic dynamics of the coupled memristive model, which are not visible in the classical case. So, the model (2) is superior and generalizable than the classical model.

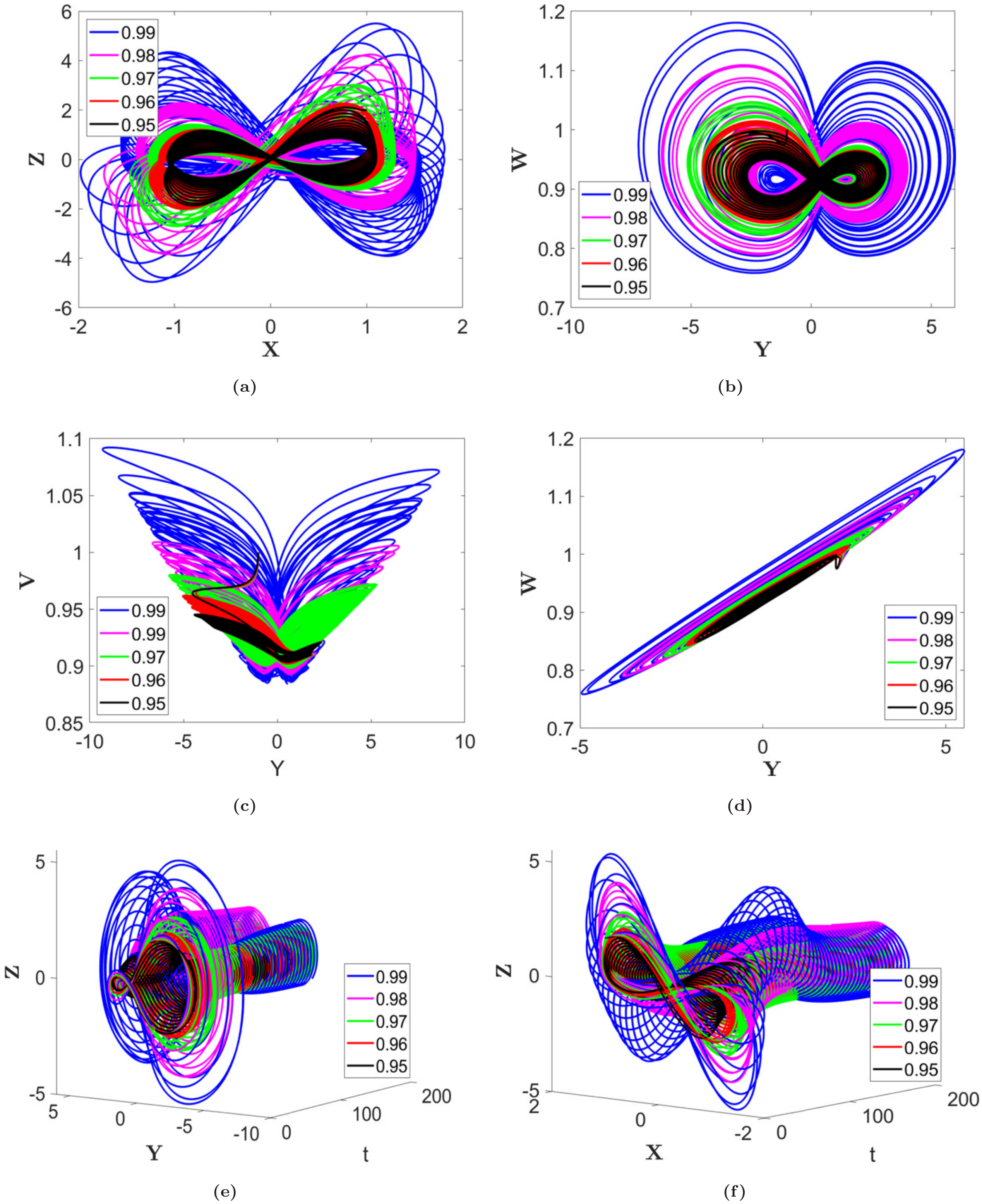

Fig. 8 The behaviors of different state variables of system (2) with different ϱ and fixed fractional order $\varpi = 0.98$.

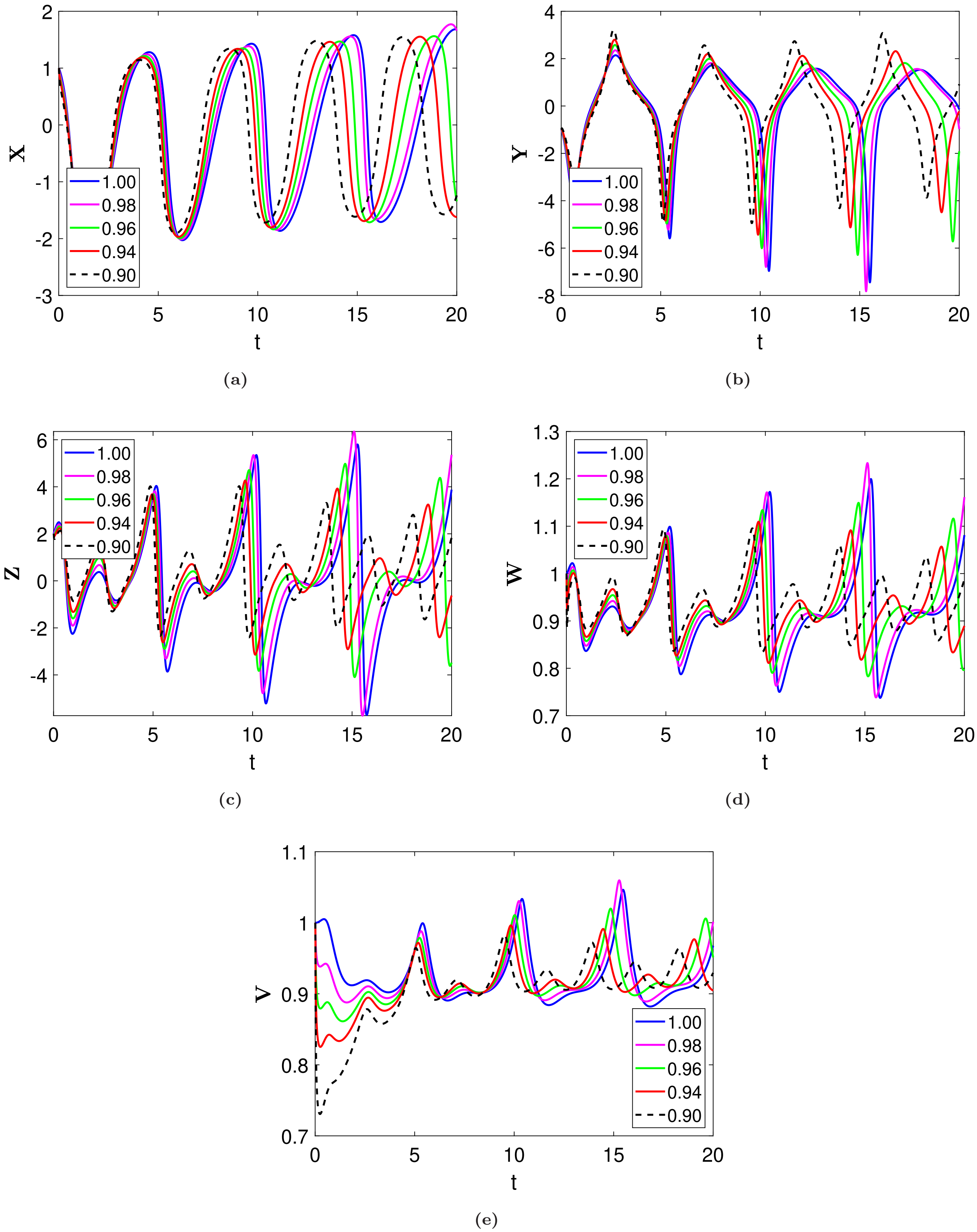

Fig. 9 The behaviors of different state variables of system (2) versus time t with different ϖ and fractal dimension $\varrho = 0.99$.

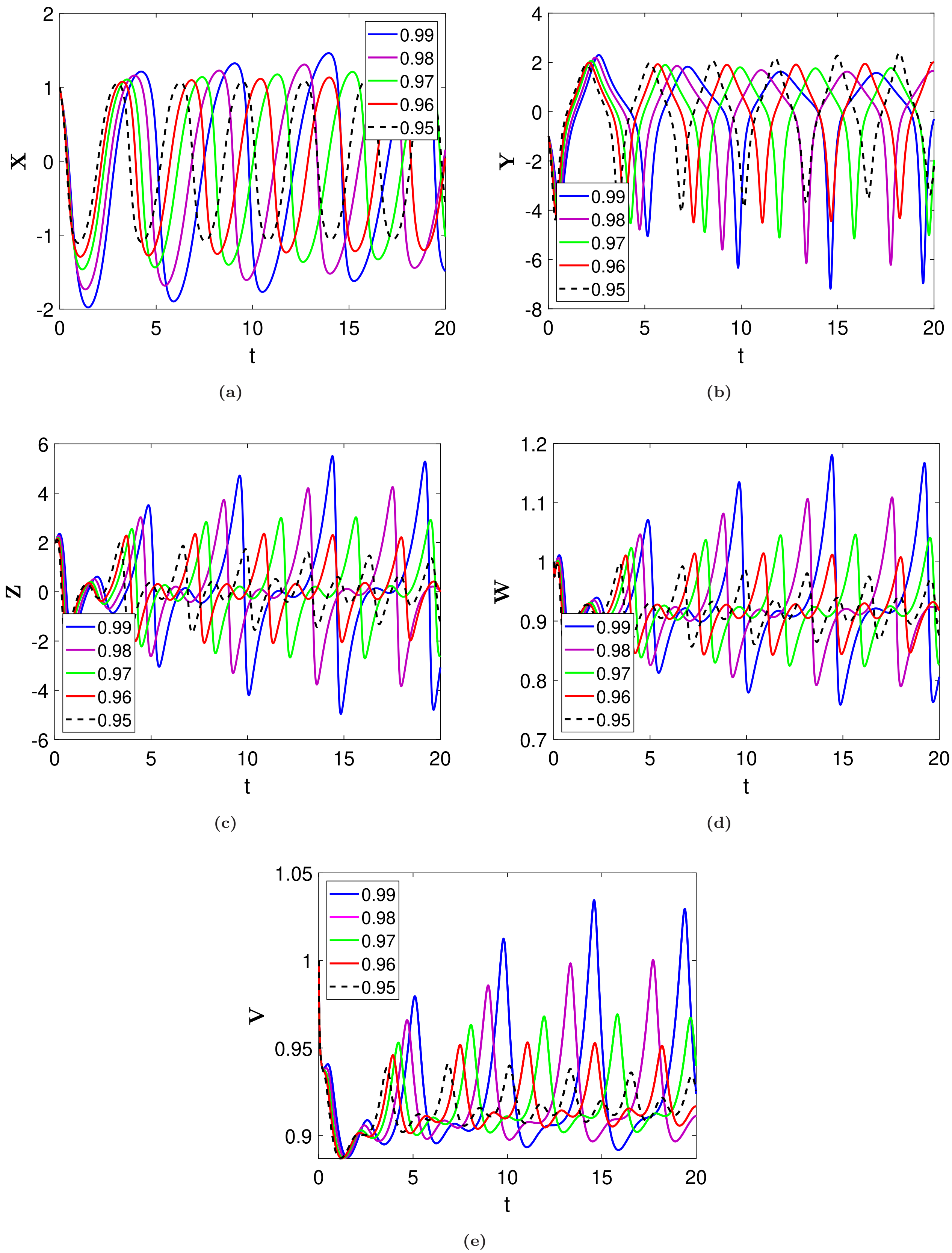

Fig. 10 The behaviors of different state variables of system (2) versus time t with different ϱ and fractional order $\varpi = 0.98$.

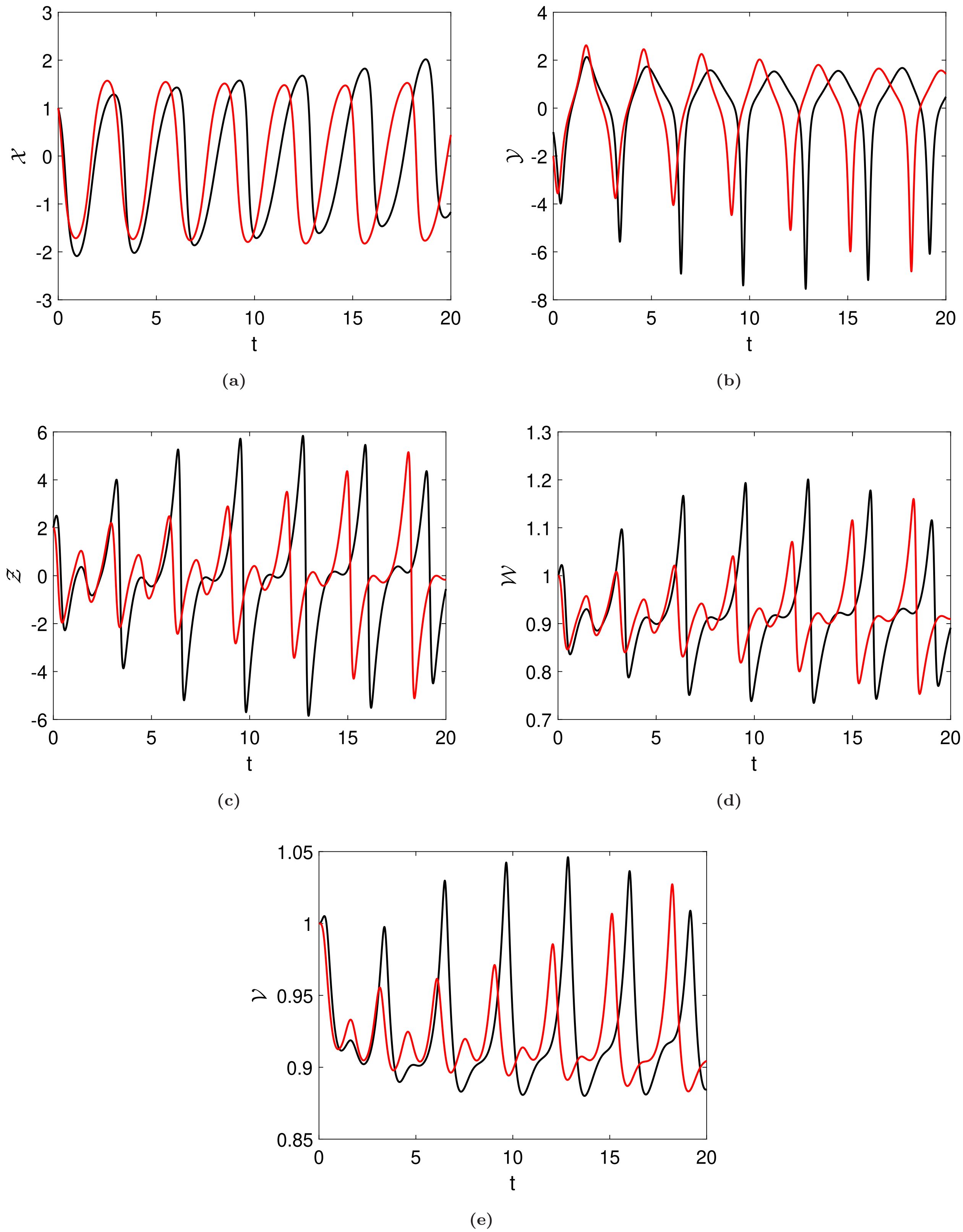

Fig. 11 The sensitive dependence of different state variables of system (2) on the initial conditions: (i) black ($[\mathbb{X}, \mathbb{Y}, \mathbb{Z}, \mathbb{W}, \mathbb{V}] = [1, -1, 2, 1, 1]$) and (ii) red ($[\mathbb{X}, \mathbb{Y}, \mathbb{Z}, \mathbb{W}, \mathbb{V}] = [1, -1.4, 2, 1, 1]$).

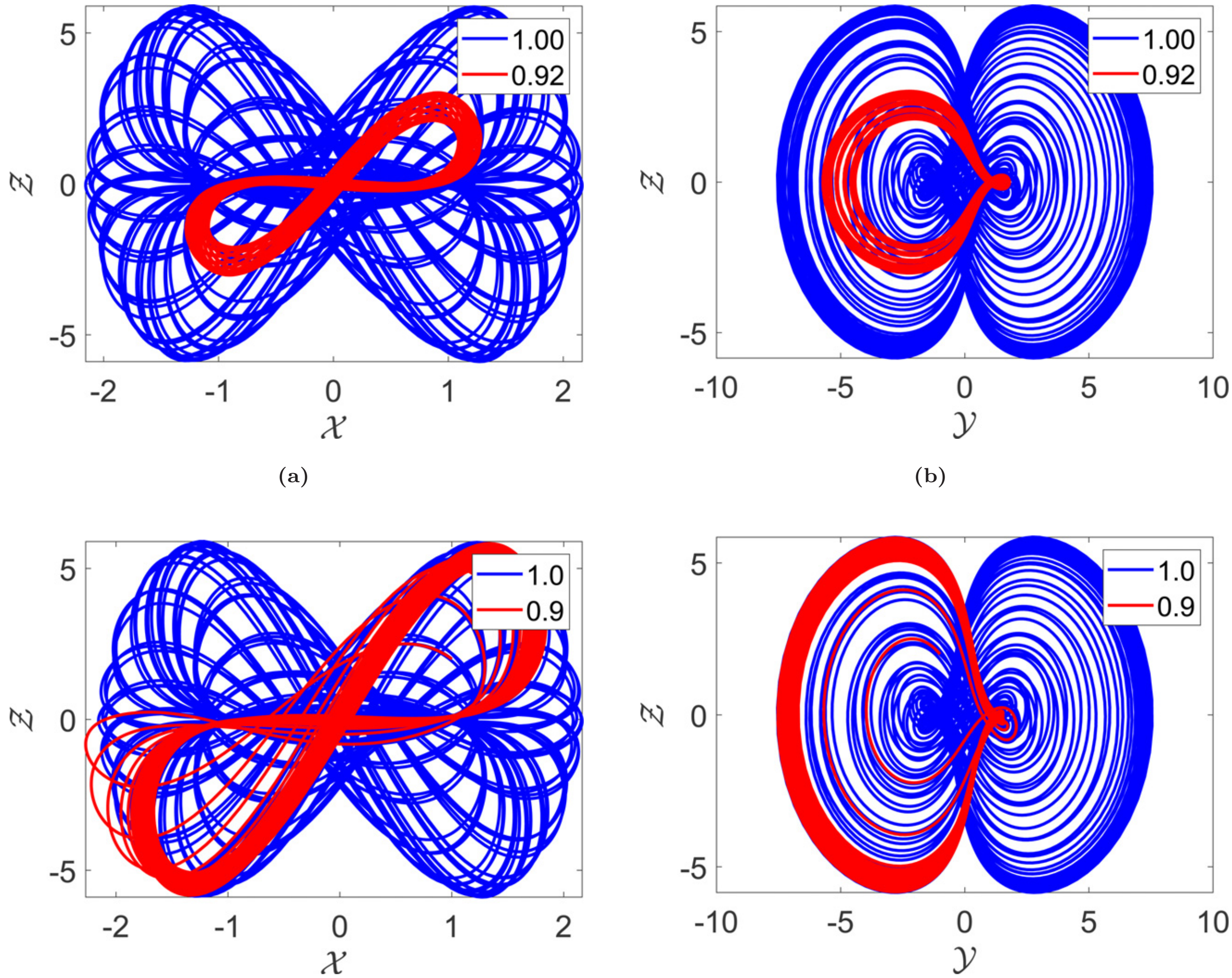

(c) (d)

Fig. 12 Comparison between some phase portraits of classical model (1) and the considered model (2).

7. CONCLUSION

In this paper, we studied a coupled memristive model in the framework of fractal–fractional derivative involving the Mittag-Leffler kernel. The existence as well as uniqueness of the solution are presented utilizing the fixed point theorems. Different properties of the system are also analyzed including dissipation, Poincaré section, phase portraits, and time-series behaviors. The dissipation property shows that the suggested system is dissipative as long as the parameter $g > 0$. Similarly, from the Poincaré section it is observed that, lowering the value of the fractal dimension, an asymmetric attractor emerges in the system. Further, we conclude that the fractional order shows a significant impact on the dynamics which reduces the extreme complex nature of the suggested model. Similarly, from the time-series analysis it is observed that at lower fractional orders and fractal dimensions, the system evolves into a limit-cycle attractor, which attracts all the trajectories toward it.

ACKNOWLEDGMENTS

The authors express their gratitude to Princess Nourah bint Abdulrahman University Researchers Supporting Project (Grant No. PNURSP2022R61), Princess Nourah bint Abdulrahman University, Riyadh, Saudi Arabia.

ORCID

S. Ahmad https://orcid.org/0000-0002-5610-6248
F. Jarad https://orcid.org/0000-0002-3303-0623

REFERENCES

1. Y. Wang, G. Wang, Y. Shen and H. H.-C. Iu, A memristor neural network using synaptic plasticity and its associative memory, *Circuits Syst. Signal Process.* **39**(7) (2020) 3496–3511.
2. A. Serb, A. Corna, R. George, A. Khiat, F. Rocchi, M. Reato, M. Maschietto, C. Mayr, G. Indiveri, S. Vassanelli and T. Prodromakis, Memristive synapses connect brain and silicon spiking neurons, *Sci. Rep.* **10**(1) (2020) 1–7.
3. F. Yu, Z. A. Zhang, L. Liu, H. Shen, Y. Y. Huang, C. Q. Shi, S. Cai, Y. Song, S. C. Du and Q. Xu, Secure communication scheme based on a new 5D multistable four-wing memristive hyperchaotic system with disturbance inputs, *Complexity* **2020**(1) (2020) 5859273.
4. H. G. Wu, Y. Ye, M. Chen, Q. Xu and B. C. Bao, Extremely slow passages in low-pass filter-based memristive oscillator, *Nonlinear Dyn.* **97**(4) (2019) 2339–2353.
5. Z. Wang, Z. Zhang and Q. Bi, Bursting oscillations with delayed C-bifurcations in a modified Chua's circuit, *Nonlinear Dyn.* **100**(3) (2020) 2899–2915.
6. F. Geng, X.-B. Lin and X. Liu, Chaotic traveling wave solutions in coupled Chua's circuits, *J. Dyn. Differ. Equ.* **31**(3) (2019) 1373–1396.
7. C. Zheng, H. H.-C. Iu, T. Fernando, D. Yu, H. Guo and J. K. Eshraghian, Analysis and generation of chaos using compositely connected coupled memristors, *Chaos* **28**(6) (2018) 063115.
8. J. Ma, P. Zhou, B. Ahmad, G. Ren and C. Wang, Chaos and multi-scroll attractors in RCL-shunted junction coupled Jerk circuit connected by memristor, *PLoS ONE* **13**(1) (2018) e0191120.
9. M. Chen, M. Sun, H. Bao, Y. Hu and B. Bao, Flux-charge analysis of two-memristor-based Chua's circuit: Dimensionality decreasing model for detecting extreme multistability, *IEEE Trans. Ind. Electron.* **67**(3) (2020) 2197–2206.
10. B. C. Bao, T. Jiang, G. Wang, P. Jin, H. Bao and M. Chen, Two-memristor-based Chua's hyperchaotic circuit with plane equilibrium and its extreme multistability, *Nonlinear Dyn.* **89**(2) (2017) 1157–1171.
11. G. A. Leonov, N. V. Kuznetsov and V. I. Vagaitsev, Localization of hidden Chua's attractors, *Phys. Lett. A* **375**(23) (2011) 2230–2233.
12. S. T. Kingni, V.-T. Pham, S. Jafari and P. Woafo, A chaotic system with an infinite number of equilibrium points located on a line and on a hyperbola and its fractional-order form, *Chaos Solitons Fractals* **99**(1) (2017) 209–218.
13. M. Chen, C. Wang, H. Bao, X. Ren, B. Bao and Q. Xu, Reconstitution for interpreting hidden dynamics with stable equilibrium point, *Chaos Solitons Fractals* **140**(1) (2020) 110188.
14. L. C. Liu, C. H. Du, X. F. Zhang, J. Li and S. S. Shi, Dynamics and entropy analysis for a new 4-D hyperchaotic system with coexisting hidden attractors, *Entropy* **21**(3) (2019) 287.
15. H. Wu, Y. Ye, M. Chen, Q. Xu and B. Bao, Periodically switched memristor initial boosting behaviors in memristive hypogenetic jerk system, *IEEE Access* **7**(1) (2019) 145022–145029.
16. D. Ding, H. Liu, Y. Weng and N. Wang, Dynamics analysis of a fractional-order delayed SBT memristive chaotic system without equilibrium points, *Eur. Phys. J. Plus* **134**(9) (2019) 444.
17. H.-M. Li, Y.-F. Yang, Y. Zhou, C.-L. Li, K. Qian, Z.-Y. Li and J.-R. Du, Dynamics and synchronization of a memristor-based chaotic system with no equilibrium, *Complexity* **2019**(1) (2019) 4647608.
18. C. Du, L. Liu, Z. Zhang and S. Yu, A coupling method of double memristors and analysis of extreme transient behavior, *Nonlinear Dyn.* **104**(1) (2021) 765–787.
19. S. Saifullah, A. Ali, M. Irfan and K. Shah, Time-fractional Klein–Gordon equation with solitary/shock waves solutions, *Math. Probl. Eng.* **2021** (2021) 6858592.
20. S. Ahmad, A. Ullah, M. Partohaghighi, S. Saifullah, A. Akgül and F. Jarad, Oscillatory and complex behaviour of Caputo–Fabrizio fractional order HIV-1 infection model, *AIMS Math.* **7**(3) (2022) 4778–4792.
21. S. Ahmad, A. Ullah, A. Akgül and M. De la Sen, A study of fractional order Ambartsumian equation involving exponential decay kernel, *AIMS Math.* **6** (2021) 9981–9997.
22. A. Atangana, Fractal–fractional differentiation and integration: Connecting fractal calculus and fractional calculus to predict complex system, *Chaos solitons Fractals* **102** (2017) 396–406.
23. S. Saifullah *et al.*, Investigation of fractal fractional nonlinear Drinfeld–Sokolov–Wilson system with non-singular operators, *Results Phys.* **33** (2022) 105145, doi:10.1016/j.rinp.2021.105145.
24. M. Aslam, M. Farman, H. Ahmad, T. N. Gia, A. Ahmad and S. Askar, Fractal fractional derivative on chemistry kinetics hires problem, *AIMS Math.* **7**(1) (2021) 1155–1184.
25. S. Saifullah, A. Ali and E. F. D. Goufo, Investigation of complex behaviour of fractal fractional chaotic attractor with Mittag-Leffler kernel, *Chaos Solitons Fractals* **152** (2021) 111332.
26. S. Ahmad, A. Ullah, A. Akgül and T. Abdeljawad, Chaotic behavior of Bhalekar–Gejji dynamical system under Atangana–Baleanu fractal fractional operator, *Fractals* **30**(1) (2022) 2240005.

27. L. Zhang, S. Ahmad, A. Ullah, A. Akgül and E. K. Akgül, Analysis of hidden attractors of non-equilibrium fractal–fractional chaotic system with one signum function, *Fractals* **30**(5) (2022) 2240139.
28. Z. Ahmad, F. Ali, N. Khan and I. Khan, Dynamics of fractal–fractional model of a new chaotic system of integrated circuit with Mittag-Leffler kernel, *Chaos Solitons Fractals* **153**(2) (2021) 111602.
29. Y. Pan, Nonlinear analysis of a four-dimensional fractional hyper-chaotic system based on general Riemann–Liouville–Caputo fractal–fractional derivative, *Nonlinear Dyn.* **106** (2021) 3615–3636.
30. A. Atangana, Modelling the spread of COVID-19 with new fractal–fractional operators: Can the lockdown save mankind before vaccination? *Chaos Solitons Fractals* **136** (2020) 109860.
31. A. Atangana and S. I. Araz, *New Numerical Scheme with Newton Polynomial*: *Theory*, *Methods*, *and Applications* (Elsevier Science, 2021).